

## A STATIC CONDENSATION REDUCED BASIS ELEMENT METHOD: APPROXIMATION AND A *POSTERIORI* ERROR ESTIMATION

DINH BAO PHUONG HUYNH<sup>1</sup>, DAVID J. KNEZEVIC<sup>1,2</sup> AND ANTHONY T. PATERA<sup>1</sup>

**Abstract.** We propose a new reduced basis element-cum-component mode synthesis approach for parametrized elliptic coercive partial differential equations. In the Offline stage we construct a Library of interoperable parametrized reference *components* relevant to some family of problems; in the Online stage we instantiate and connect reference components (at ports) to rapidly form and query parametric *systems*. The method is based on static condensation at the interdomain level, a conforming eigenfunction “port” representation at the interface level, and finally Reduced Basis (RB) approximation of Finite Element (FE) bubble functions at the intradomain level. We show under suitable hypotheses that the RB Schur complement is close to the FE Schur complement: we can thus demonstrate the stability of the discrete equations; furthermore, we can develop inexpensive and rigorous (system-level) *a posteriori* error bounds. We present numerical results for model many-parameter heat transfer and elasticity problems with particular emphasis on the Online stage; we discuss flexibility, accuracy, computational performance, and also the effectivity of the *a posteriori* error bounds.

**Mathematics Subject Classification.** 35J25, 65N30, 65D99.

Received May 25, 2011. Revised November 24, 2011.  
Published online November 23, 2012.

### 1. INTRODUCTION

The Reduced Basis Element (RBE) method is a computational approach for the approximation of partial differential equations which combines domain decomposition with parametric model order reduction. In particular, the “classical” RBE method typically appeals to nonconforming approaches – mortar [24] or Discontinuous Galerkin [9] – at the interdomain level and then Reduced Basis (RB) approximation [28] at the intradomain level. The RBE method enjoys several advantages relative to the standard “mono-domain” RB method: we are never required to solve the truth Finite Element (FE) problem over the full domain – we may thus address very large problems; we pursue many RB approximations over low dimensional parameter spaces rather than a single RB approximation over a very high dimensional parameter space – we may thus consider *many* parameters, as well as more general geometries and topologies. Also, related ideas for viscous fluid flows have been developed in the RB hybrid element approach of [19]. The RBE method is particularly efficient for problems which might contain

---

*Keywords and phrases.* Reduced Basis method, Reduced Basis Element method, domain decomposition, Schur complement, elliptic partial differential equations, *a posteriori* error estimation, component mode synthesis, parametrized systems.

<sup>1</sup> Department of Mechanical Engineering, Massachusetts Institute of Technology, Cambridge, 02139 MA, USA. [huynh@mit.edu](mailto:huynh@mit.edu)

<sup>2</sup> School of Engineering and Applied Sciences, Harvard University, Cambridge, 02138 MA, USA.  
[dknezevic@seas.harvard.edu](mailto:dknezevic@seas.harvard.edu); [patera@mit.edu](mailto:patera@mit.edu)

many repeated subdomains as in this case a single intradomain RB preparation can be shared by all similar subdomains. Reduced basis element approximations can also be integrated with finite element approximations over regions of the domain not readily amenable to model reduction [1, 2].

In this paper we develop a static condensation RBE approach: we consider standard static condensation at the interdomain level and then RB approximation of the requisite “bubble” functions (and associated Schur complement entries) at the intradomain level. This approach extends the reach of the classical RBE in several important ways. First, in the classical RBE approach the RB spaces for a particular subdomain – which we may view as a “component” – must be aware of neighboring subdomains: components are not generally interchangeable or interoperable and hence the analysis process is “top-down” from system to components. In contrast, in our static condensation RBE approach, the RB space for a particular component is designed to reflect all possible function variations on the component interfaces (which we shall denote “ports”): components are thus completely interchangeable and interoperable and the analysis is “bottom-up” from a library of components to many possible systems. (A similar component interchangeability is achieved in [12], based on an integral equation formulation of the RB, for electromagnetic scattering problems). Second, in the classical mortar RBE approach, the computation of *a posteriori* error bounds necessitates appeal to the intradomain truth FE approximation in order to correct for jump terms. In contrast, in our (conforming) static condensation RBE approach, the *a posteriori* error bounds may be computed solely in terms of interface degrees of freedom and intradomain RB quantities – in essence, at very little additional cost relative to the field and output prediction.

It follows from these advantages that the static condensation RBE provides for a more favorable Offline-Online decomposition than either the standard RB method or the classical RBE approach. The Offline stage is performed once: we prepare, for each component in a library, the RB bubble spaces and collateral RB data required to populate the approximate Schur complement. The Online stage is then performed many times: we may assemble any system – we require only compatibility of ports – from multiple instantiations of components from the library; we then compute the system field and outputs, and associated *a posteriori* error bounds, for different values of the parameter in a prescribed parameter domain. The operation count and storage requirement for the Online stage depends only on the number of interface degrees of freedom and the dimension of the intradomain RB spaces. In summary, the Online stage of the static condensation RBE is much more flexible than the Online stage for the standard RB method, in which the system is already assembled and only parametric variations are permitted, as well as the Online stage of the classical RBE method, in which the RB intradomain spaces already reflect anticipated connectivity. The “bottom up” approach and associated Online flexibility is particularly attractive in interactive design environments, in real-time parameter estimation contexts, and more generally in discovery and optimization processes.

These advantages do of course come at some cost: increased degrees of freedom on ports (which we recall are the interfaces between the components). The RB spaces associated with the classical RBE approach reflect connectivity and thus relatively few port (Lagrange multiplier) degrees of freedom are required to ensure continuity; in contrast, in the static condensation RBE method, we must (in effect) reflect in our RB spaces any behavior of the solution over the ports. In order to minimize this parasitic effect we choose a particular interface representation (and associated lifting into the interior of the components) which (i) respects the relevant trace theorems and FE Schur complement theory [7] to ensure a stable discretization, (ii) leads to relatively economical RB spaces for the intradomain bubbles, and finally, (iii) permits, through a hierarchical approach, subsequent (adaptive) Online economization of port degrees of freedom, as pursued in [11]. In some cases we may pursue in (iii) a more Draconian economization in the spirit of the classical RBE approach; indeed, in the quasi-one-dimensional limit we may even consider a single degree of freedom on each port [4].

Our approach is also closely related to the multiscale Reduced Basis Method (MsRBM) proposed in [26] (see also a more recent MsRBM proposal [21]). The macroscale discretization of the MsRBM corresponds to the “system” in our static condensation RBE approach, and the microscale or cell of the MsRBM corresponds to the “component” in the static condensation RBE approach. In the MsRBM the emphasis is thus on many and more homogeneous macroscale elements with a very simple treatment of the macroscale-microscale interface; in contrast, in the static condensation RBE approach, we will typically address relatively fewer but more

heterogeneous components for which we must include a *general* interface representation. Nevertheless, there are many similarities between the MsRBM and the static condensation RBE method, and indeed the MsRBM can perhaps take advantage of the system-level *a posteriori* error bounds developed in the current paper to bound the error between the MsRBM and associated truth MsFEM [16].

In the above we discuss the provenance of the static condensation RBE from the reduced basis perspective. However, our approach is also quite similar to the Component Mode Synthesis (CMS) approaches which are in widespread and very effective use in industry for many years. These CMS approaches are first proposed in the seminal papers [10, 17], but there is much subsequent development, refinement, and applications. As in the static condensation RBE method, the CMS approach combines static condensation at the interdomain level with model order reduction at the intradomain level. In the earlier work [10, 17] the CMS model order reduction is typically of the intradomain eigenfunction modal truncation variety, however more recently Krylov spaces are also considered [14] as well as spaces relevant to MsFEM approaches [15].

In our approach we directly adopt the CMS anatomy, vocabulary – components and ports – and even strategy, however we replace the intradomain modal model order reduction with RB model order reduction. This substitution can offer several advantages within the parametric context: from an approximation perspective, our approach will provide rapid convergence [5, 8, 25] over an entire parametric solution manifold compared to typically algebraic convergence of the CMS modal expansion [6, 15]; from a computational perspective, we amortize the expensive construction of the reduced order model over many system analyses (corresponding to different parameter values from the prescribed parameter domain). In short, our approach provides greater flexibility in the inexpensive Online stage: interchangeability of components is extended to include parametric variations which arise in geometry, constitutive laws, and sources and loads. Furthermore, in the static condensation RBE approach, *a posteriori* error bounds for the RB approximations at the component level permit us to develop *a posteriori* error bounds at the system level without recourse to the truth FE residual over the full domain [14, 20]. We should note that in this paper we consider only elliptic coercive partial differential equations and not the more difficult eigenproblems or dynamic problems to which CMS approaches are typically applied.

In Section 2 we pose the symmetric coercive second-order partial differential equation for which we shall develop our approach. In Section 3 we introduce the truth approximation which we wish to accelerate: a fine FE discretization defined (but, in our approach, never invoked) over the full domain. Finally, we develop the static condensation formulation of the truth FE discretization; we focus on the treatment of the interface degrees of freedom. In Section 4 we develop the static condensation RBE and we prove the well-posedness of the static condensation RBE approximation based on stability estimates developed in Brenner [7]. In Section 5 we develop the static condensation RBE system level *a posteriori* error estimates: we combine standard RB error estimates at the component level with matrix perturbation analysis [13] of the approximate Schur complement at the system level. We demonstrate that our error estimates are strict upper bounds for the actual error between the static condensation RBE approximation and the underlying truth FE discretization. In Section 6 we discuss the Offline and Online computational procedures and provide detailed operation counts and storage requirements for the Online stage in particular. Finally, in Section 7 we present numerical results for a scalar field problem (heat transfer) and a vector field problem (linear elasticity); we report the accuracy and computational cost for different representative systems and we discuss the quality of the *a posteriori* error bounds.

## 2. CONTINUOUS PROBLEM: COMPONENTS AND SYSTEMS

### 2.1. Physical domain formulation

We first introduce a set or library of regions, which we shall denote “archetype component” domains,  $\hat{\Omega}_m^o(\hat{\mu}_m^{\text{geo}})$ ,  $1 \leq m \leq M$ , for geometry parameters  $\hat{\mu}_m^{\text{geo}}$ . The  $m$ th archetype component has  $\hat{P}_m^{\text{geo}}$  geometric parameters, which reside in an associated geometry parameter domain  $\hat{D}_m^{\text{geo}} \subset \mathbb{R}^{\hat{P}_m^{\text{geo}}}$ . For each archetype component domain  $\hat{\Omega}_m^o(\hat{\mu}_m^{\text{geo}})$  we further identify elements of the boundary,  $\hat{\gamma}_{m,j}^o(\hat{\mu}_m^{\text{geo}})$ ,  $1 \leq j \leq n_m^\gamma$  (where  $n_m^\gamma \geq 1$ ), which we shall denote “archetype component port” domains. We require for simplicity that the intersection

of any two ports in any given archetype component is empty; this “mutually disjoint port” condition may be relaxed, as we discuss further below. Here the  $\hat{\cdot}$  indicates archetype and the  $^o$  refers to a quantity defined over the physical domain (we will later introduce reference domains).

We associate to each of these archetype component domains bilinear and linear forms: for  $w, v \in H^1(\hat{\Omega}_m^o(\hat{\mu}_m^{\text{geo}}))$ , we define  $\hat{a}_m^o(w, v; \hat{\mu}_m^{\text{coeff}}; \hat{\mu}_m^{\text{geo}})$ ,  $\hat{f}_m^o(v; \hat{\mu}_m^{\text{coeff}}; \hat{\mu}_m^{\text{geo}})$ ,  $\hat{\ell}_m^o(v; \hat{\mu}_m^{\text{coeff}}; \hat{\mu}_m^{\text{geo}})$ ,  $1 \leq m \leq M$ , for coefficient parameters  $\hat{\mu}_m^{\text{coeff}}$  in associated coefficient parameter domains  $\hat{\mathcal{D}}_m^{\text{coeff}} \in \mathbb{R}^{\hat{P}_m^{\text{coeff}}}$ . Note that the forms  $\hat{a}_m^o(w, v; \hat{\mu}_m^{\text{coeff}}; \hat{\mu}_m^{\text{geo}})$  and  $\hat{f}_m^o(v; \hat{\mu}_m^{\text{coeff}}; \hat{\mu}_m^{\text{geo}})$  will define the PDE weak form, and  $\hat{\ell}_m^o(v; \hat{\mu}_m^{\text{coeff}}; \hat{\mu}_m^{\text{geo}})$  will define the output functional. (These bilinear and linear forms may include trace terms over  $\partial\hat{\Omega}_m^o(\hat{\mu}_m^{\text{geo}})$ ). We also define for future reference  $\hat{\mathcal{D}}_m \equiv \hat{\mathcal{D}}_m^{\text{geo}} \times \hat{\mathcal{D}}_m^{\text{coeff}}$ ,  $1 \leq m \leq M$ ;  $\hat{\mathcal{D}}_m$  is the parameter domain (both geometry and coefficient) for the  $m$ th archetype component. Also, we let  $\hat{\mu}_m \equiv (\hat{\mu}_m^{\text{geo}}, \hat{\mu}_m^{\text{coeff}}) \in \hat{\mathcal{D}}_m$  denote the parameters for the  $m$ th archetype component. Recall also that for any domain  $\mathcal{O}$  in  $\mathbb{R}^d$ ,  $H^1(\mathcal{O}) \equiv \{v \in L^2(\mathcal{O}) : \nabla v \in (L^2(\mathcal{O}))^d\}$ , where  $L^2(\mathcal{O}) \equiv \{v \text{ measurable over } \mathcal{O} : \int_{\mathcal{O}} v^2 \text{ finite}\}$ .

We next introduce “instantiated component” domains,  $\Omega_i^o(\mu_i^{\text{geo}}) = \hat{\Omega}_{\mathcal{M}(i)}^o(\mu_i^{\text{geo}})$ ,  $1 \leq i \leq I$ , where  $\mathcal{M}$  is a mapping from  $\{1, \dots, I\}$  (component instantiations) to  $\{1, \dots, M\}$  (component archetypes). The corresponding instantiated component port domains, also denoted more succinctly as “local ports,” are thus given by  $\gamma_{i,j}^o(\mu_i^{\text{geo}}) = \hat{\gamma}_{\mathcal{M}(i),j}^o(\mu_i^{\text{geo}})$ ,  $1 \leq j \leq n_{\mathcal{M}(i)}^{\gamma}$ . Here  $\mu^{\text{geo}} \equiv (\mu_1^{\text{geo}}, \dots, \mu_I^{\text{geo}}) \in \mathcal{D}^{\text{geo}}$ , where  $\mathcal{D}^{\text{geo}}$  is a subset of  $\prod_{i=1}^I \hat{\mathcal{D}}_{\mathcal{M}(i)}^{\text{geo}}$  which ensures that a geometric compatibility requirement (defined below) is satisfied (as well as any problem-specific constraints on parameters). Note these instantiated components no longer bear the  $\hat{\cdot}$  of the archetype components but retain the  $^o$  associated with the physical domain. For future reference we also define  $\mathcal{D}^{\text{coeff}} \equiv \prod_{i=1}^I \hat{\mathcal{D}}_{\mathcal{M}(i)}^{\text{coeff}}$ . Also, we set  $\mu \equiv (\mu^{\text{geo}}, \mu^{\text{coeff}}) \in \mathcal{D} \equiv \mathcal{D}^{\text{geo}} \times \mathcal{D}^{\text{coeff}}$ .

We now consider a “system domain”  $\Omega^o(\mu^{\text{geo}})$  which is the union of instantiated component domains,

$$\overline{\Omega}^o(\mu^{\text{geo}}) = \bigcup_{i=1}^I \overline{\Omega}_i^o(\mu_i^{\text{geo}}).$$

Our geometric compatibility requirement states that,

- (i) the instantiated component domains must not intersect;
- (ii)  $\overline{\Omega}_i^o(\mu_i^{\text{geo}}) \cap \overline{\Omega}_{i'}^o(\mu_{i'}^{\text{geo}})$  must either be empty or an entire local port in each of the two (distinct) instantiated component domains  $i$  and  $i'$ ;<sup>3</sup> and
- (iii) the system connectivity as reflected in the local port connections must remain fixed for all  $\mu \in \mathcal{D}^{\text{geo}}$ .

It is important to note that geometric parameters define either “internal” geometric transformations of a component (such as dilation or shear), or “rigid body” transformations (translations, rotations). Both types of geometric parameters affect the geometric compability of our system domain. For future reference, we refer to the “rigid body” transformation parameters as “docking parameters.”

We may now also define a set of global ports  $\Gamma_p^o(\mu^{\text{geo}})$ ,  $1 \leq p \leq n^{\Gamma}$ : each global port is either the intersection (in fact, coincidence) of two local ports or a local port on  $\partial\Omega^o(\mu^{\text{geo}})$ . We illustrate in Figure 1 two archetype components with associated local port domains as well as a system of three instantiated component domains with associated global port domains. We can summarize the port connections with index sets  $\pi_p$ ,  $1 \leq p \leq n^{\Gamma}$ , which for the case of a global port corresponding to (coincidence of) two local ports  $\gamma_{i',j'}^o, \gamma_{i'',j''}^o$  takes the form  $\pi_p = \{(i', j'), (i'', j'')\}$  and for the case of a global port corresponding to a single local port  $\gamma_{i',j'}^o$  takes the form  $\pi_p = \{(i', j')\}$ . We can also define a local to global port index mapping  $\mathcal{G}$  such that  $\pi_p = \{(i', j'), (i'', j'')\}$  is equivalent to  $p = \mathcal{G}_{i'}(j') = \mathcal{G}_{i''}(j'')$ ; this mapping is invertible for a given instantiated component such that  $j' = \mathcal{G}_{i'}^{-1}(p)$  and  $j'' = \mathcal{G}_{i''}^{-1}(p)$ . We observe from the geometric compatibility condition (iii) that the sets  $\pi_p$ ,  $1 \leq p \leq n^{\Gamma}$ , and the mapping  $\mathcal{G}$  do not depend on  $\mu \in \mathcal{D}^{\text{geo}}$ .

<sup>3</sup>Note that in the case of an arbitrarily thin crack between two instantiated components we must interpret the respective instantiated component domains to be separated by an arbitrarily small gap such that the closures do not in fact intersect.

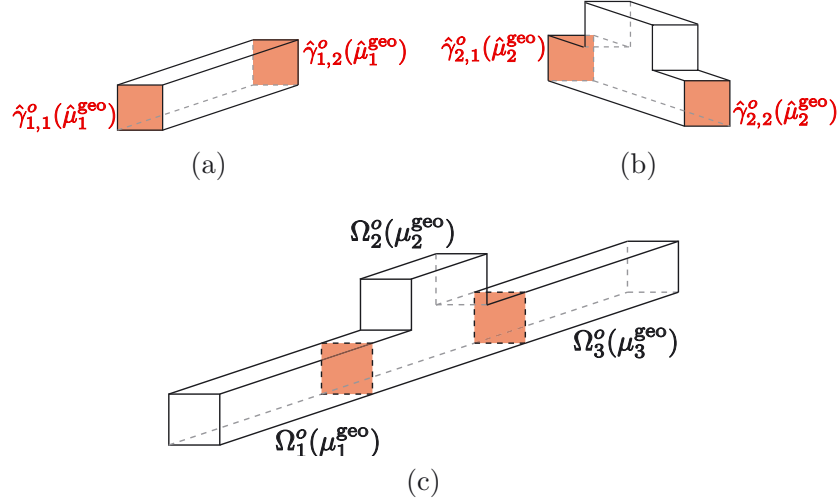


FIGURE 1. (a) An archetype component,  $\hat{\Omega}_1^o(\hat{\mu}_1^{\text{geo}})$ , with two local ports indicated in red. (b) An archetype component,  $\hat{\Omega}_2^o(\hat{\mu}_2^{\text{geo}})$ , with two local ports. (c) A system of three instantiated component domains with associated global port domains.

We may now introduce a global function space  $X^o(\mu^{\text{geo}}) \equiv \{v^o \in H^1(\Omega^o(\mu^{\text{geo}})) : v^o|_{\partial\Omega_D^o(\mu^{\text{geo}})} = 0\}$  where  $\partial\Omega_D^o(\mu^{\text{geo}})$  represents the part of the system domain boundary over which we impose homogeneous Dirichlet conditions (note inhomogeneous Dirichlet conditions are readily treated by appropriate lifting functions). We shall assume for simplicity that  $\partial\Omega_D^o(\mu^{\text{geo}})$  is the union of (at least one) entire instantiated component port domains. We endow  $X^o(\mu^{\text{geo}})$  with an inner product  $(\cdot, \cdot)_{X^o(\mu^{\text{geo}})}$  and induced norm  $\|\cdot\|_{X^o(\mu^{\text{geo}})}$ .

It is then natural to form the system bilinear and linear forms, defined with respect to  $X^o(\mu^{\text{geo}})$ , in terms of the corresponding archetype component forms introduced earlier. In particular, for all  $w^o, v^o \in X^o(\mu^{\text{geo}})$ , we introduce

$$a^o(w^o, v^o; \mu) = \sum_{i=1}^I \hat{a}_{\mathcal{M}(i)}^o(w^o|_{\Omega_i^o(\mu_i^{\text{geo}})}, v^o|_{\Omega_i^o(\mu_i^{\text{geo}})}; \mu_i^{\text{coeff}}; \mu_i^{\text{geo}}), \quad (2.1)$$

$$f^o(v^o; \mu) = \sum_{i=1}^I \hat{f}_{\mathcal{M}(i)}^o(v^o|_{\Omega_i^o(\mu_i^{\text{geo}})}; \mu_i^{\text{coeff}}; \mu_i^{\text{geo}}), \quad (2.2)$$

$$\ell^o(v^o; \mu) = \sum_{i=1}^I \hat{\ell}_{\mathcal{M}(i)}^o(v^o|_{\Omega_i^o(\mu_i^{\text{geo}})}; \mu_i^{\text{coeff}}; \mu_i^{\text{geo}}). \quad (2.3)$$

We may then introduce coercivity and continuity constants for  $\mu \in \mathcal{D}$ ,

$$\alpha^o(\mu) \equiv \inf_{v^o \in X^o(\mu^{\text{geo}})} \frac{a^o(v^o, v^o; \mu)}{\|v^o\|_{X^o(\mu^{\text{geo}})}^2}, \quad (2.4)$$

$$\gamma^{o,\text{cont}}(\mu) \equiv \sup_{v^o \in X^o(\mu^{\text{geo}})} \sup_{w^o \in X^o(\mu^{\text{geo}})} \frac{a^o(v^o, w^o; \mu)}{\|v^o\|_{X^o(\mu^{\text{geo}})} \|w^o\|_{X^o(\mu^{\text{geo}})}}. \quad (2.5)$$

We shall assume that there exists  $\alpha_0 > 0$  and finite  $\gamma_0^{\text{cont}}$  such that  $\alpha^o(\mu) \geq \alpha_0$  and  $\gamma^{o,\text{cont}}(\mu) \leq \gamma_0^{\text{cont}}$  for all  $\mu \in \mathcal{D}$ . We also assume that our linear functionals are bounded over  $X^o(\mu^{\text{geo}})$ .

We may now state the system problem. Given  $\mu \in \mathcal{D}$ : find the field  $u^o(\mu) \in X^o(\mu^{\text{geo}})$  such that

$$a^o(u^o(\mu), v^o; \mu) = f^o(v^o; \mu), \quad \forall v^o \in X^o(\mu^{\text{geo}}); \quad (2.6)$$

evaluate the system output of interest  $s(\mu) = \ell^o(u^o(\mu); \mu)$ . Under the assumptions on coercivity and continuity this problem is well posed by the Lax–Milgram theorem.

## 2.2. Reference domain formulation

For our subsequent reduced basis treatment we shall require a fixed reference domain for each archetype component (and hence associated instantiated components). We take this reference domain to be  $\Omega_m \equiv \hat{\Omega}_m^o(\hat{\mu}_m^{\text{geo,ref}})$  for some  $\hat{\mu}_m^{\text{geo,ref}} \in \hat{\mathcal{D}}_m^{\text{geo}}$ ; we denote the corresponding archetype component reference port domains as  $\gamma_{m,j}$ ,  $1 \leq j \leq n_m^\gamma$ . Note that these reference archetype domains and reference archetype port domains implicitly bear a  $\hat{\cdot}$  and a superscript  $\text{ref}$ ; for simplicity, in particular since we will almost exclusively work with the reference quantities in what follows, we instead use the absence of the superscript  $^o$  to indicate an archetype and reference (rather than physical) domain.

We then suppose [28] that there exists a piecewise affine (invertible) mapping  $\mathcal{A}_m(\cdot; \hat{\mu}_m^{\text{geo}})$  such that  $\hat{\Omega}_m^o(\hat{\mu}_m^{\text{geo}}) = \mathcal{A}_m(\Omega_m; \hat{\mu}_m^{\text{geo}})$  for all  $\hat{\mu}_m^{\text{geo}} \in \hat{\mathcal{D}}_m^{\text{geo}}$ . Also, we introduce the constants  $\rho^{\mathcal{A}}(\mu^{\text{geo}})$  and  $\rho_{\text{LB}}^{\mathcal{A}} > 0$ , where

$$\rho^{\mathcal{A}}(\mu^{\text{geo}}) \equiv \min_{\substack{1 \leq i \leq I \\ 1 \leq j \leq n_{\mathcal{M}(i)}^\gamma}} \frac{\rho(\gamma_{i,j}^o(\mu_i^{\text{geo}}))}{\rho(\gamma_{\mathcal{M}(i),j})} \geq \rho_{\text{LB}}^{\mathcal{A}}, \quad \forall \mu^{\text{geo}} \in \mathcal{D}^{\text{geo}}. \quad (2.7)$$

Here, for a domain  $\gamma \subset \mathbb{R}^{d-1}$ ,  $\rho(\gamma)$  denotes the diameter of the largest  $(d-1)$ -dimensional ball that can be contained within  $\gamma$ . Hence (2.7) simply implies that our geometric map is not “degenerate” on any of the ports.

Note that our geometric compatibility condition (ii) implies that for any two instantiated components  $i'$  and  $i''$  which share a port,  $\Gamma_p^o(\mu^{\text{geo}}) = \gamma_{i',j'}^o(\mu_{i'}^{\text{geo}}) = \gamma_{i'',j''}^o(\mu_{i''}^{\text{geo}})$ ,

$$\mathcal{A}_{\mathcal{M}(i')}(\gamma_{\mathcal{M}(i'),j'}; \mu_{i'}^{\text{geo}}) = \mathcal{A}_{\mathcal{M}(i'')}(\gamma_{\mathcal{M}(i''),j''}; \mu_{i''}^{\text{geo}}).$$

This condition provides a practical means to verify that the geometric compatibility condition (ii) is satisfied.

We may now express our space  $X^o(\mu^{\text{geo}})$  as

$$X^o(\mu^{\text{geo}}) = \{v^o \in L^2(\Omega^o(\mu^{\text{geo}})) : v^o|_{\Omega_i^o(\mu_i^{\text{geo}})} = [v]_i \circ (\mathcal{A}_{\mathcal{M}(i)}(\cdot; \mu_i^{\text{geo}}))^{-1}, 1 \leq i \leq I, \forall v \in X\},$$

where  $v \equiv [v_1, \dots, v_I]$  and

$$\begin{aligned} X \equiv \{ & [v_1, \dots, v_I] : \text{for } i = 1, \dots, I, [v]_i \in H^1(\Omega_{\mathcal{M}(i)}); \\ & [v]_{i'}|_{\gamma_{\mathcal{M}(i'),j'}} = [v]_{i''}|_{\gamma_{\mathcal{M}(i''),j''}} \text{ for } \gamma_{i',j'}^o(\mu_{i'}^{\text{geo}}) = \gamma_{i'',j''}^o(\mu_{i''}^{\text{geo}}); \\ & [v]_i|_{\gamma_{\mathcal{M}(i),j}} = 0 \text{ for } \gamma_{i,j}^o \in \partial\Omega_D^o(\mu^{\text{geo}})\}, \end{aligned}$$

is a parameter-independent space. (We can express the space  $X$  without reference to any parameters but to avoid complicated notation we prefer the choice above in which parameter-dependent quantities serve to implicitly define parameter-independent indicial relations). Note it is the continuity condition on the ports in  $X$  which ensures that  $X^o(\mu^{\text{geo}}) \subset H^1(\Omega^o(\mu^{\text{geo}}))$ . In what follows we shall let  $\mathcal{W}(\mu^{\text{geo}}) : X \rightarrow X^o(\mu^{\text{geo}})$  denote the one-to-one transformation between a function  $v^o \in X^o(\mu^{\text{geo}})$  and its pre-image  $v \in X$  – hence  $v^o = \mathcal{W}(\mu^{\text{geo}})v$ . Note we define  $[v]_i$  to be the  $i$ th component of  $v \in X$ . We also let  $\{\mathbf{e}_i, 1 \leq i \leq I\}$  denote the canonical basis of  $\mathbb{R}^I$ , such that say  $[v]_3 \mathbf{e}_3 = [0, 0, [v]_3, 0, \dots]$ .

For each archetype reference component  $m$ ,  $1 \leq m \leq M$ , we introduce an inner product,  $(\cdot, \cdot)_{X_m}$ , on  $H^1(\Omega_m)$  and we let  $\|\cdot\|_{X_m}$  denote the corresponding induced norm. In fact – to anticipate subsequent developments with regard to *bubble spaces* – we shall only require that  $\|\cdot\|_{X_m}$  is a *semi-norm* on  $H^1(\Omega_m)$ , but that it is a full norm on  $\{v \in H^1(\Omega) : v|_{\gamma_{m,j}} = 0, 1 \leq j \leq n_m^\gamma\}$ . We then define the inner product and norm for  $v, w \in X$  as

$$(w, v)_X \equiv \sum_{i=1}^I ([w]_i, [v]_i)_{X_{\mathcal{M}(i)}}, \quad \|v\|_X \equiv \sqrt{(v, v)_X}. \quad (2.8)$$

Due to the one-to-one correspondence between  $X$  and  $X^o(\mu^{\text{geo}})$ , (2.8) also provides an inner product and norm on  $X^o(\mu^{\text{geo}})$ , and we shall henceforth suppose that

$$(w^o, v^o)_{X^o(\mu^{\text{geo}})} = (\mathcal{W}(\mu^{\text{geo}})^{-1}w^o, \mathcal{W}(\mu^{\text{geo}})^{-1}v^o)_X, \quad \forall v^o, w^o \in X^o(\mu^{\text{geo}}), \quad (2.9)$$

$$\|v^o\|_{X^o(\mu^{\text{geo}})} = \|\mathcal{W}(\mu^{\text{geo}})^{-1}v^o\|_X, \quad \forall v^o \in X^o(\mu^{\text{geo}}), \quad (2.10)$$

define the inner products and norms over  $X^o(\mu^{\text{geo}})$  introduced formally earlier.

We may now introduce archetype component bilinear and linear forms defined over the *reference* domains as  $\hat{\mu}_m \equiv (\hat{\mu}_m^{\text{geo}}, \hat{\mu}_m^{\text{coeff}}) \in \hat{\mathcal{D}}_m \rightarrow a_m(w, v; \hat{\mu}_m), f_m(v; \hat{\mu}_m), \ell_m(w, v; \hat{\mu}_m), 1 \leq m \leq M$ , where for all  $w, v \in H^1(\Omega_m)$ ,

$$\begin{aligned} a_m(w, v; \hat{\mu}_m) &= \hat{a}_m^o(w \circ (\mathcal{A}_m(\cdot; \hat{\mu}_m^{\text{geo}}))^{-1}, v \circ (\mathcal{A}_m(\cdot; \hat{\mu}_m^{\text{geo}}))^{-1}; \hat{\mu}_m^{\text{coeff}}; \hat{\mu}_m^{\text{geo}}), \\ f_m(v; \hat{\mu}_m) &= \hat{f}_m^o(v \circ (\mathcal{A}_m(\cdot; \hat{\mu}_m^{\text{geo}}))^{-1}; \hat{\mu}_m^{\text{coeff}}; \hat{\mu}_m^{\text{geo}}), \\ \ell_m(v; \hat{\mu}_m) &= \hat{\ell}_m^o(v \circ (\mathcal{A}_m(\cdot; \hat{\mu}_m^{\text{geo}}))^{-1}; \hat{\mu}_m^{\text{coeff}}; \hat{\mu}_m^{\text{geo}}). \end{aligned}$$

We reiterate here that the absence of any  $^o$  or  $\hat{\cdot}$  symbols in the forms introduced above means that these are archetype reference quantities. Note that these reference-domain bilinear and linear forms now depend on both the geometric and coefficient parameters and in fact the former will now also appear as ‘‘coefficients’’ which reflect the change of variables.

It is important to note that, under modest assumptions [28] on  $\hat{a}_m^o(\cdot, \cdot; \hat{\mu}_m^{\text{coeff}}; \hat{\mu}_m^{\text{geo}}), \hat{f}_m^o(\cdot; \hat{\mu}_m^{\text{coeff}}; \hat{\mu}_m^{\text{geo}})$ , and  $\hat{\ell}_m^o(\cdot; \hat{\mu}_m^{\text{coeff}}; \hat{\mu}_m^{\text{geo}})$ , it follows from our piecewise-affine hypothesis on the mappings  $\mathcal{A}_m$  that the  $a_m(\cdot, \cdot; \hat{\mu}_m), f_m(\cdot; \hat{\mu}_m)$ , and  $\ell_m(\cdot; \hat{\mu}_m)$  are affine in functions of parameter in the sense that

$$a_m(w, v; \hat{\mu}_m) = \sum_{q=1}^{Q_{a_m}} \Theta_{a_m}^q(\hat{\mu}_m) a_m^q(w, v) \quad (2.11)$$

with similar representations for  $f_m$  and  $\ell_m$ . We shall denote by  $Q_{\max}$  the maximum of  $Q_{a_m}, Q_{f_m}$ , and  $Q_{\ell_m}$  over all  $m = 1, \dots, M$ .

We may then further define, for  $w = [w_1, \dots, w_I] \in X, v = [v_1, \dots, v_I] \in X$ , and  $\mu \in \mathcal{D}$ ,

$$\begin{aligned} a(w, v; \mu) &= \sum_{i=1}^I a_{\mathcal{M}(i)}([w]_i, [v]_i; \mu_i), \\ f(v; \mu) &= \sum_{i=1}^I f_{\mathcal{M}(i)}([v]_i; \mu_i), \\ \ell(v; \mu) &= \sum_{i=1}^I \ell_{\mathcal{M}(i)}([v]_i; \mu_i), \end{aligned}$$

where  $\mu_i \equiv (\mu_i^{\text{geo}}, \mu_i^{\text{coeff}})$  for  $(\mu_1^{\text{geo}}, \mu_2^{\text{geo}}, \dots, \mu_I^{\text{geo}}; \mu_1^{\text{coeff}}, \mu_2^{\text{coeff}}, \dots, \mu_I^{\text{coeff}}) \in \mathcal{D}$ .

We may now rewrite our system equations in terms of reference-domain quantities. For given  $\mu \in \mathcal{D}$ : find  $u(\mu) \in X$  such that

$$a(u(\mu), v; \mu) = f(v; \mu), \quad \forall v \in X; \quad (2.12)$$

evaluate the system output of interest as

$$s(\mu) = \ell(u(\mu); \mu). \quad (2.13)$$

It is readily demonstrated that  $u^o(\mu) = \mathcal{W}(\mu^{\text{geo}})u(\mu)$ . These reference-domain equations will be our point of departure for subsequent discretization. (As required for visualization of numerical results we shall invoke  $u^o$  over  $\Omega^o(\mu^{\text{geo}})$ ).

Also, from the definitions above, it follows that the coercivity and continuity constants associated with (2.12) are given by

$$\begin{aligned}\alpha(\mu) &\equiv \inf_{v \in X} \frac{a(v, v; \mu)}{\|v\|_X^2} = \inf_{v^\circ \in X^\circ(\mu^{\text{geo}})} \frac{a^\circ(v^\circ, v^\circ; \mu)}{\|v^\circ\|_{X^\circ(\mu^{\text{geo}})}^2} = \alpha^\circ(\mu), \\ \gamma^{\text{cont}}(\mu) &\equiv \sup_{v \in X} \sup_{w \in X} \frac{a(v, w; \mu)}{\|v\|_X \|w\|_X} = \sup_{v^\circ \in X^\circ(\mu^{\text{geo}})} \sup_{w^\circ \in X^\circ(\mu^{\text{geo}})} \frac{a^\circ(v^\circ, w^\circ; \mu)}{\|v^\circ\|_{X^\circ(\mu^{\text{geo}})} \|w^\circ\|_{X^\circ(\mu^{\text{geo}})}} = \gamma^{\circ, \text{cont}}(\mu),\end{aligned}$$

and hence (2.12) inherits the well-posedness of (2.6).

### 3. FINITE ELEMENT TRUTH FORMULATION

#### 3.1. Discrete spaces

We now introduce finite element approximation spaces  $X_m^h$  over the archetype component reference domains  $\Omega_m$ ,  $1 \leq m \leq M$ . For each  $m$ , the spaces  $X_m^h$  are endowed with the inner-product and induced norm,  $(\cdot, \cdot)_{X_m}$  and  $\|\cdot\|_{X_m}$ , from Section 2. We may also define port spaces  $P_{m,j}^h$ : for any  $w \in X_m^h$  there exists a  $v \in P_{m,j}^h$  such that  $v = w|_{\gamma_{m,j}}$ . We set  $\mathcal{N}_{m,j}^\gamma \equiv \dim(P_{m,j}^h)$ .

We require our spaces to collectively satisfy a port discretization compatibility (conforming) condition: for any doubleton port connection set,  $\pi_p = \{(i', j'), (i'', j'')\}$ , and for any  $v \in P_{\mathcal{M}(i'), j'}^h$ , there exists  $w \in P_{\mathcal{M}(i''), j''}^h$  such that  $v \circ \mathcal{A}_{\mathcal{M}(i')}^{-1}(\gamma_{\mathcal{M}(i'), j'}; \mu_{i'}^{\text{geo}}) = w \circ \mathcal{A}_{\mathcal{M}(i'')}^{-1}(\gamma_{\mathcal{M}(i''), j''}; \mu_{i''}^{\text{geo}})$ ,  $\forall \mu^{\text{geo}} \in \mathcal{D}^{\text{geo}}$ . We also require an analogous condition when the roles of  $v$  and  $w$  are exchanged, and hence there is a one-to-one correspondence between  $P_{\mathcal{M}(i'), j'}^h$  and  $P_{\mathcal{M}(i''), j''}^h$ . It might appear that this condition would impose system-specific constraints on the archetype components which are intended to form many different systems. In fact, it is possible to satisfy the port discretization compatibility condition for all possible connections of various appropriate subsets of archetype components. For example, consider the case of two-dimensional archetype components with ports which are straight segments: a uniform mesh with the same number of degrees of freedom on each port will ensure that the port discretization compatibility condition will be satisfied for all possible connection sets.

In subsequent developments we shall extensively employ finite element *bubble spaces*. The bubble spaces on the archetype reference domains are given by

$$B_{m;0}^h \equiv \{v \in X_m^h : v|_{\gamma_{m,j}} = 0, 1 \leq j \leq n_m^\gamma\}, \quad 1 \leq m \leq M, \quad (3.1)$$

and we have associated coercivity and continuity constants

$$\alpha_{m;0}^h(\hat{\mu}_m) \equiv \inf_{v \in B_{m;0}^h} \frac{a_m(v, v; \hat{\mu}_m)}{\|v\|_{X_m}^2}, \quad (3.2)$$

$$\gamma_{m;0}^{h, \text{cont}}(\hat{\mu}_m) \equiv \sup_{v \in B_{m;0}^h} \sup_{w \in B_{m;0}^h} \frac{a_m(v, w; \hat{\mu}_m)}{\|v\|_{X_m} \|w\|_{X_m}}. \quad (3.3)$$

These constants are positive for all  $\hat{\mu}_m \in \hat{\mathcal{D}}_m$  for each archetype component – positivity of  $\alpha_{m;0}^h(\hat{\mu}_m)$  follows from our assumption that  $\|\cdot\|_{X_m}$  is a semi-norm on  $X_m^h$ , and that  $B_{m;0}^h$  has a non-empty Dirichlet boundary (since  $n_m^\gamma \geq 1$  for  $1 \leq m \leq M$ ).

The system truth finite element space is then given by  $X^h = (\oplus_{i=1}^I X_{\mathcal{M}(i)}^h) \cap X$ . (Here the intersection with  $X$  imposes our continuity conditions on the component ports). Note that for  $b_i^h \in B_{\mathcal{M}(i);0}^h$ , the  $I$ -tuple  $b_i^h \mathbf{e}_i$  is in  $X^h$  due to the condition that bubble functions vanish on ports. The associated *system truth* coercivity and



continuity constants are given by

$$\alpha^h(\mu) \equiv \inf_{v \in X^h} \frac{a(v, v; \mu)}{\|v\|_X^2}, \quad (3.4)$$

$$\gamma^{h, \text{cont}}(\mu) \equiv \sup_{v \in X^h} \sup_{w \in X^h} \frac{a(v, w; \mu)}{\|v\|_X \|w\|_X}. \quad (3.5)$$

We note that since  $X^h \subset X$ , we have  $\alpha(\mu) \leq \alpha^h(\mu)$  and  $\gamma^{h, \text{cont}}(\mu) \leq \gamma^{\text{cont}}(\mu)$ .

The truth discretization may now be stated. Given  $\mu \in \mathcal{D}$ : find  $u^h(\mu) \in X^h$  such that

$$a(u^h(\mu), v; \mu) = f(v; \mu), \quad \forall v \in X^h; \quad (3.6)$$

evaluate the system output of interest,

$$s^h(\mu) = \ell(u^h(\mu); \mu). \quad (3.7)$$

The formulation (3.6), (3.7) is well-posed due to our conditions on  $\alpha^h(\mu)$  and  $\gamma^{h, \text{cont}}(\mu)$ . We shall build our reduced basis element approximation upon this truth discretization, and we shall measure the error in our reduced basis element approximation relative to this truth discretization.

### 3.2. Static condensation

To prepare for static condensation we must construct a basis for our truth approximation (which in fact will be inherited by our reduced basis element method).

First, we introduce an eigenfunction basis for each port space,  $P_{m,j}^h$ ,  $1 \leq j \leq n_m^\gamma$ ,  $1 \leq m \leq M$ . In particular, for a given port (*i.e.*  $m, j$  fixed), we introduce the eigenfunction basis  $\{\chi_{m,j,k} \in P_{m,j}^h : 1 \leq k \leq \mathcal{N}_{m,j}^\gamma\}$ . These eigenfunctions are associated with the discrete generalized eigenvalue problem

$$\int_{\gamma_{m,j}} \nabla \chi_{m,j,k} \cdot \nabla v = \lambda_{m,j,k} \int_{\gamma_{m,j}} \chi_{m,j,k} v, \quad \forall v \in P_{m,j}^h, \quad (3.8)$$

$$\|\chi_{m,j,k}\|_{L^2(\gamma_{m,j})} = 1; \quad (3.9)$$

here the  $\lambda_{m,j,k} \in \mathbb{R}$  denote real positive eigenvalues ordered such that  $(\lambda_{\min} \equiv) \lambda_{m,j,1} < \lambda_{m,j,2} < \dots < \lambda_{m,j,\mathcal{N}_{m,j}^\gamma}$ . Note that rather than the simple Laplacian inner product we might consider an energy inner product or even more beneficially a singular Sturm–Liouville problem [11] to ensure more rapid decay [3, 6] of the modal amplitudes (for purposes of truncation). It follows from (3.8), (3.9) that the  $\chi_{m,j,k}$  satisfy the orthonormality property

$$(\chi_{m,j,k'}, \chi_{m,j,k''})_{L^2(\gamma_{m,j})} = \delta_{k'k''}, \quad 1 \leq k', k'' \leq \mathcal{N}_{m,j}^\gamma, \quad (3.10)$$

where  $\delta_{ij}$  denotes the Kronecker delta function. For treatment of more general port topologies which do not honor the mutually disjoint port assumption we would need to introduce “wire-basket” representations such as developed in [15].

The port eigenmodes are then elliptically lifted to the interior of the archetype reference domain to yield  $\psi_{m,j,k} \in X_m^h$ ,  $1 \leq j \leq n_m^\gamma$ ,  $1 \leq m \leq M$ ,  $1 \leq k \leq \mathcal{N}_{m,j}^\gamma$ . We construct  $\psi_{m,j,k}$  such that it satisfies the Laplace equation on the component interior, coincides with  $\chi_{m,j,k}$  on  $\gamma_{m,j,k}$ , and vanishes on the remaining ports,

$$\int_{\Omega_m} \nabla \psi_{m,j,k} \cdot \nabla v = 0, \quad \forall v \in B_{m;0}^h, \quad (3.11)$$

$$\psi_{m,j,k} = \chi_{m,j,k}, \quad \text{on } \gamma_{m,j}, \quad (3.12)$$

$$\psi_{m,j,k} = 0, \quad \text{on } \gamma_{m,j'}, \quad \forall j' \in \{1, \dots, j-1, j+1, \dots, n_m^\gamma\}. \quad (3.13)$$

We have employed the Laplacian in (3.11), but of course other elliptic operators are also possible. Also, we emphasize that in (3.8) and (3.11) we are referring to the Laplacian operator in  $\mathbb{R}^{d-1}$  and  $\mathbb{R}^d$ , respectively.

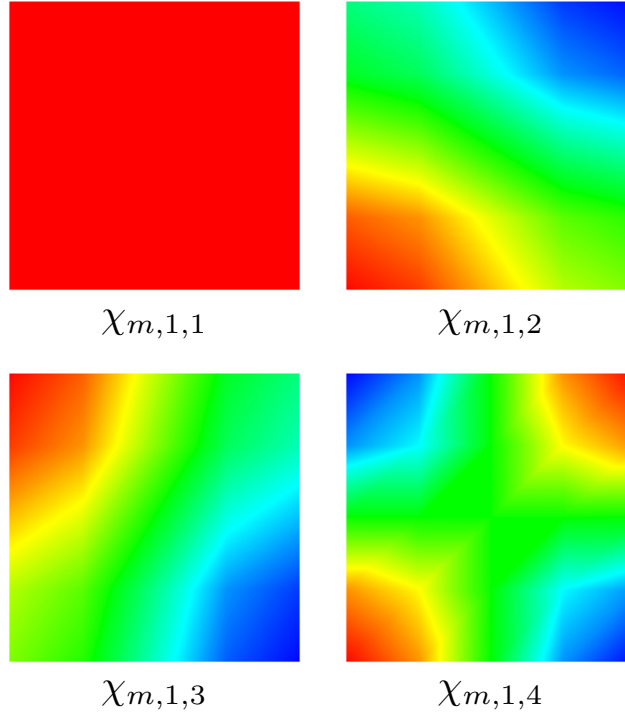


FIGURE 2. The first four modes of the eigenproblem (3.8), (3.9) for port  $\gamma_{m,1}$  of a archetype reference component  $\Omega_m$ . Here  $\gamma_{m,1}$  is a square port  $(0, 0.4)^2$  with a uniform  $4 \times 4$  Q1 ( $d = 2$ ) mesh.

For purposes of illustration we consider an archetype reference component  $\Omega_m \equiv (0, 0.4) \times (0, 0.4) \times (0, 3)$ , with truth space  $X_m^h$  meshed with  $4 \times 4 \times 30$   $Q_1$  ( $d = 3$ ) elements; the component has two square ports,  $\gamma_{m,1} \equiv (0, 0.4) \times (0, 0.4) \times \{0\}$  and  $\gamma_{m,2} \equiv (0, 0.4) \times (0, 0.4) \times \{3\}$ , perforce each meshed with uniform  $4 \times 4$   $Q_1$  ( $d = 2$ ) elements. Figure 2 presents the first four eigenmodes for  $\gamma_{m,1}$ ; Figure 3 shows the result of lifting these four port eigenmodes to the interior of the parallelepiped component.

We comment on the choice of eigenexpansion: orthonormality will ensure stability in appropriate norms [7]; hierarchy will permit possible modal truncation [3, 11, 20]; modal structure will ensure rapid decay of lifting functions into the component interior (as demonstrated in Fig. 3) and ultimately more rapid RB convergence. We will return to this latter point subsequently in the context of our numerical examples.

We have defined interface functions local to archetype reference domains; we shall also require interface functions lifted over instantiated components connected to a global port. We denote the latter by  $\Psi_{p,k} \in X^h$ ,  $1 \leq k \leq \mathcal{N}_p^T$ ,  $1 \leq p \leq n^T$ ; the  $\Psi_{p,k}$  are indexed by the global port number,  $p$ , and the port mode number,  $k$ . Also,  $\mathcal{N}_p^T$  denotes the number of port modes on global port  $\Gamma_p^o(\mu^{\text{geo}})$ , where  $\pi_p = \{(i', j'), (i'', j'')\}$ , and hence  $\mathcal{N}_p^T \equiv \mathcal{N}_{\mathcal{M}(i', j')}^\gamma = \mathcal{N}_{\mathcal{M}(i'', j'')}^\gamma$ . We prefer to define the  $\Psi_{p,k}$  with respect to our reference domains, and thus we construct the  $\Psi_{p,k}$  as  $I$ -tuples: for an interior port  $\pi_p = \{(i', j'), (i'', j'')\}$ , and for port mode  $k$  (where  $1 \leq k \leq \mathcal{N}_p^T$ ),  $\Psi_{p,k} = \psi_{\mathcal{M}(i'), j', k} \mathbf{e}_{i'} + \psi_{\mathcal{M}(i''), j'', k} \mathbf{e}_{i''} \in X^h$ . Similarly, for a boundary port  $\pi_p = \{(i', j')\}$ , and for port mode  $k$ ,  $\Psi_{p,k} = \psi_{\mathcal{M}(i'), j', k} \mathbf{e}_{i'}$ . As in Section 2, we can map  $\Psi_{p,k} \in X^h$  to the system domain *via*  $\mathcal{W}(\mu^{\text{geo}})$ .

We now discuss the static condensation procedure which we employ to eliminate the degrees of freedom internal to each component. First, it is clear that we can express  $u^h(\mu) \in X^h$  in terms of bubble and interface

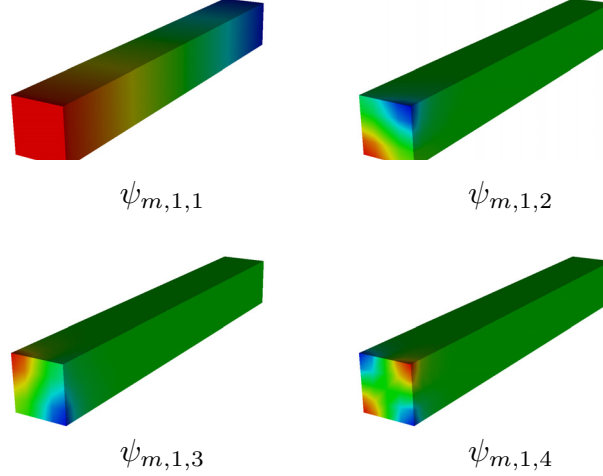


FIGURE 3. The elliptically lifted interface functions (3.11)–(3.13) corresponding to the modes in Figure 2 on a “stem” archetype reference component  $(0, 0.4)^2 \times (0, 3)$  with two square ports.

contributions as

$$u^h(\mu) = \sum_{i=1}^I b_i^h(\mu) \mathbf{e}_i + \sum_{p=1}^{n^r} \sum_{k=1}^{\mathcal{N}_p^r} U_{p,k}(\mu) \Psi_{p,k}, \quad (3.14)$$

where  $b_i^h(\mu) \in B_{\mathcal{M}(i);0}^h$ . Here,  $U_{p,k}(\mu)$ ,  $1 \leq p \leq n^r$ ,  $1 \leq k \leq \mathcal{N}_p^r$ , are interface function coefficients.

Now, since  $b_i^h(\mu) \mathbf{e}_i \in X^h$ , we can eliminate bubble functions from (3.6) in favor of global port degrees of freedom. To wit, we substitute (3.14) into (3.6) and test on  $v \mathbf{e}_i$ , for  $v \in B_{\mathcal{M}(i);0}^h$ , to obtain,

$$a_{\mathcal{M}(i)} \left( b_i^h(\mu) + \sum_{j=1}^{n_{\mathcal{M}(i)}^\gamma} \sum_{k=1}^{\mathcal{N}_{\mathcal{M}(i),j}^\gamma} U_{\mathcal{G}_i(j),k}(\mu) \psi_{\mathcal{M}(i),j,k}(v; \mu_i) \right) = f_{\mathcal{M}(i)}(v; \mu_i), \quad \forall v \in B_{\mathcal{M}(i);0}^h. \quad (3.15)$$

Recall that  $\mathcal{G}$  is a local to global port index mapping such that  $\pi_p = \{(i', j'), (i'', j'')\}$  is equivalent to  $p = \mathcal{G}_{i'}(j') = \mathcal{G}_{i''}(j'')$ . It follows that  $b_i^h(\mu) \in B_{\mathcal{M}(i);0}^h$  satisfies,

$$a_{\mathcal{M}(i)}(b_i^h(\mu), v; \mu_i) = f_{\mathcal{M}(i)}(v; \mu_i) - \sum_{j=1}^{n_{\mathcal{M}(i)}^\gamma} \sum_{k=1}^{\mathcal{N}_{\mathcal{M}(i),j}^\gamma} U_{\mathcal{G}_i(j),k}(\mu) a_{\mathcal{M}(i)}(\psi_{\mathcal{M}(i),j,k}(v; \mu_i), \quad \forall v \in B_{\mathcal{M}(i);0}^h, \quad (3.16)$$

for each  $1 \leq i \leq I$ . The existence and uniqueness of  $b_i^h(\mu)$  from (3.16) is guaranteed due to coercivity (and continuity) of  $a_{\mathcal{M}(i)}(\cdot, \cdot; \mu_i)$  on  $B_{\mathcal{M}(i);0}^h$ .

From (3.16) and linearity, we can reconstruct  $b_i^h(\mu)$  as

$$b_i^h(\mu) = b_i^{f;h}(\mu_i) + \sum_{j=1}^{n_{\mathcal{M}(i)}^\gamma} \sum_{k=1}^{\mathcal{N}_{\mathcal{M}(i),j}^\gamma} U_{\mathcal{G}_i(j),k}(\mu) b_{i,j,k}^h(\mu_i), \quad (3.17)$$

where  $b_i^{f;h}(\mu_i) \in B_{\mathcal{M}(i);0}^h$  satisfies

$$a_{\mathcal{M}(i)}(b_i^{f;h}(\mu_i), v; \mu_i) = f_{\mathcal{M}(i)}(v; \mu_i), \quad \forall v \in B_{\mathcal{M}(i);0}^h, \quad (3.18)$$

and the  $b_{i,j,k}^h(\mu_i) \in B_{\mathcal{M}(i);0}^h$  are defined by the set of  $\mathcal{N}_{\mathcal{M}(i)}^{\text{ports}}$  subproblems

$$a_{\mathcal{M}(i)}(b_{i,j,k}^h(\mu_i), v; \mu_i) = -a_{\mathcal{M}(i)}(\psi_{\mathcal{M}(i),j,k}, v; \mu_i), \quad \forall v \in B_{\mathcal{M}(i);0}^h, \quad (3.19)$$

where  $\mathcal{N}_m^{\text{ports}} \equiv \sum_{j=1}^{n_m^\gamma} \mathcal{N}_{m,j}^\gamma$ ,  $m = 1, \dots, M$ . Both (3.18) and (3.19) are well-posed again thanks to coercivity and continuity of  $a_{\mathcal{M}(i)}(\cdot, \cdot; \mu_i)$  over  $B_{\mathcal{M}(i);0}^h$ .

For  $1 \leq p \leq n^\Gamma$  and  $1 \leq k \leq \mathcal{N}_p^\Gamma$ , let

$$\Phi_{p,k}(\mu) \equiv \Psi_{p,k} + \sum_{(i',j') \in \pi_p} b_{i',j',k}^h(\mu_{i'}) \mathbf{e}_{i'} = \sum_{(i',j') \in \pi_p} (\psi_{i',j',k} + b_{i',j',k}^h(\mu_{i'})) \mathbf{e}_{i'}. \quad (3.20)$$

Also, we define the ‘‘skeleton space’’

$$X_S^h(\mu) \equiv \text{span}\{\Phi_{p,k}(\mu) : 1 \leq p \leq n^\Gamma, 1 \leq k \leq \mathcal{N}_p^\Gamma\} \cap X^h, \quad (3.21)$$

where we intersect with  $X$  in order to impose Dirichlet boundary conditions. The skeleton space  $X_S^h(\mu)$  is endowed with the inner product and norm,

$$(v, w)_{S^o} \equiv \sum_{p=1}^{n^\Gamma} (\mathcal{W}(\mu^{\text{geo}})v, \mathcal{W}(\mu^{\text{geo}})w)_{L^2(\Gamma_p^o(\mu^{\text{geo}}))} \quad \text{and} \quad \|v\|_{S^o} \equiv \sqrt{(v, v)_{S^o}}, \quad (3.22)$$

for any  $v, w \in X_S^h(\mu)$ . Note that we include a superscript  $o$  to emphasize that the inner product and norm are defined with respect to the physical domain.

It follows from (3.14) that on component  $i$ ,  $1 \leq i \leq I$ ,  $u^h(\mu)$  is given by

$$[u^h(\mu)]_i = b_i^h(\mu) + \sum_{j=1}^{n_{\mathcal{M}(i)}^\gamma} \sum_{k=1}^{\mathcal{N}_{\mathcal{M}(i),j}^\gamma} U_{\mathcal{G}_i(j),k}(\mu) \psi_{i,j,k}. \quad (3.23)$$

Hence, from (3.17) and (3.23), we have

$$[u^h(\mu)]_i = b_i^{f;h}(\mu_i) + \sum_{j=1}^{n_{\mathcal{M}(i)}^\gamma} \sum_{k=1}^{\mathcal{N}_{\mathcal{M}(i),j}^\gamma} U_{\mathcal{G}_i(j),k}(\mu) (\psi_{i,j,k} + b_{i,j,k}^h(\mu_i)). \quad (3.24)$$

It then follows from (3.24) and (3.20) that the global solution can be expressed as

$$u^h(\mu) = \sum_{i=1}^I b_i^{f;h}(\mu_i) \mathbf{e}_i + \sum_{p=1}^{n^\Gamma} \sum_{k=1}^{\mathcal{N}_p^\Gamma} U_{p,k}(\mu) \Phi_{p,k}(\mu). \quad (3.25)$$

We now insert (3.25) into (3.6) and restrict the test space to  $X_S^h(\mu)$  to arrive at

$$\sum_{p=1}^{n^\Gamma} \sum_{k=1}^{\mathcal{N}_p^\Gamma} U_{p,k}(\mu) a(\Phi_{p,k}(\mu), v; \mu) = f(v; \mu) - \sum_{i=1}^I a(b_{f,i}^h(\mu_i) \mathbf{e}_i, v; \mu), \quad \forall v \in X_S^h(\mu), \quad (3.26)$$

which completes the static condensation.

We now proceed to identify the linear algebraic statement associated with (3.26). In particular, we test in (3.26) on  $\Phi_{p',k'}(\mu)$  for  $1 \leq p' \leq n^\Gamma$ ,  $1 \leq k' \leq \mathcal{N}_{p'}^\Gamma$ , to obtain the static condensation system of dimension  $n_{\text{sc}} \equiv \sum_{p=1}^{n^\Gamma} \mathcal{N}_p^\Gamma$ ,

$$\mathbb{A}(\mu) \mathbb{U}(\mu) = \mathbb{F}(\mu), \quad (3.27)$$

for the vector  $\mathbb{U}(\mu) \in \mathbb{R}^{n_{\text{sc}}}$  of coefficients  $U_{p,k}(\mu)$ . We may also express our system output (3.7) as

$$s^h(\mu) \equiv (\mathbb{L}^1(\mu) + \mathbb{L}^2(\mu))^T \mathbb{U}(\mu) + \sum_{i=1}^I \ell(b_i^{f;h}(\mu_i) \mathbf{e}_i; \mu_i).$$

We now define these static condensation quantities more explicitly.

The matrix  $\mathbb{A}(\mu) \in \mathbb{R}^{n_{\text{sc}} \times n_{\text{sc}}}$  and vector  $\mathbb{F}(\mu) \in \mathbb{R}^{n_{\text{sc}}}$  are defined as

$$\mathbb{A}_{(p',k'),(p,k)}(\mu) \equiv a(\Phi_{p,k}(\mu), \Phi_{p',k'}(\mu); \mu), \quad (3.28)$$

and

$$\mathbb{F}_{p',k'}(\mu) \equiv f(\Phi_{p',k'}(\mu); \mu) - \sum_{i=1}^I a(b_i^{f;h}(\mu_i), \Phi_{p',k'}(\mu); \mu), \quad (3.29)$$

respectively, for  $1 \leq p \leq n^\Gamma$ ,  $1 \leq k \leq \mathcal{N}_p^\Gamma$ , and  $1 \leq p' \leq n^\Gamma$ ,  $1 \leq k' \leq \mathcal{N}_{p'}^\Gamma$ ; from (3.28) it is clear that  $\mathbb{A}(\mu)$  is symmetric. The output vectors  $\mathbb{L}^1(\mu) \in \mathbb{R}^{n_{\text{sc}}}$  and  $\mathbb{L}^2(\mu) \in \mathbb{R}^{n_{\text{sc}}}$  are given by

$$\mathbb{L}_{p,k}^1(\mu) \equiv \ell(\Psi_{p,k}(\mu); \mu), \quad \mathbb{L}_{p,k}^2(\mu) \equiv \sum_{(i',j') \in \pi_p} \ell(b_{i',j',k}^h(\mu_{i'}) \mathbf{e}_{i'}), \quad (3.30)$$

for  $1 \leq p \leq n^\Gamma$ ,  $1 \leq k \leq \mathcal{N}_p^\Gamma$ . To better understand the matrices and vectors  $\mathbb{A}(\mu)$  and  $\mathbb{F}(\mu)$  (a similar procedure applies to  $\mathbb{L}^1, \mathbb{L}^2$ ) we consider the assembly of the static condensation system; this assembly process, similar to finite element assembly or ‘‘stamping,’’ is crucial to the general implementation of our approach.

Let  $\mathbb{A}^i(\mu) \in \mathbb{R}^{\mathcal{N}_{\mathcal{M}(i)}^{\text{ports}} \times \mathcal{N}_{\mathcal{M}(i)}^{\text{ports}}}$  and  $\mathbb{F}^i(\mu) \in \mathbb{R}^{\mathcal{N}_{\mathcal{M}(i)}^{\text{ports}}}$  denote the ‘‘local stiffness matrix’’ and ‘‘local load vector’’ on instantiated component  $i$ , respectively, which from (3.20) has entries

$$\mathbb{A}_{(j',k'),(j,k)}^i(\mu_i) \equiv a_{\mathcal{M}(i)}(\psi_{\mathcal{M}(i),j,k} + b_{i,j,k}^h(\mu_i), \psi_{\mathcal{M}(i),j',k'} + b_{i,j',k'}^h(\mu_i); \mu_i), \quad (3.31)$$

$$\mathbb{F}_{j',k'}^i(\mu_i) \equiv f_{\mathcal{M}(i)}(\psi_{\mathcal{M}(i),j',k'} + b_{i,j',k'}^h(\mu_i); \mu_i) - a_{\mathcal{M}(i)}(b_i^{f;h}(\mu_i), \psi_{\mathcal{M}(i),j',k'} + b_{i,j',k'}^h(\mu_i); \mu_i), \quad (3.32)$$

for  $1 \leq j \leq n_{\mathcal{M}(i)}^\gamma$ ,  $1 \leq k \leq \mathcal{N}_{\mathcal{M}(i),j}^\gamma$ , and  $1 \leq j' \leq n_{\mathcal{M}(i)}^\gamma$ ,  $1 \leq k' \leq \mathcal{N}_{\mathcal{M}(i),j'}^\gamma$ . Algorithm 1 then defines the assembly procedure by which we construct (in practice) (3.28), (3.29) from (3.31), (3.32); we employ the notation ‘‘ $A \ += B$ ’’ to represent an increment ‘‘ $A \leftarrow A + B$ .’’ Note that in the case in which we require a Dirichlet condition on a port, Algorithm 1 needs a slight modification: once the assembly is complete, we *eliminate* the Dirichlet port degrees of freedom from the system. This post-processing step is analogous to the standard procedure for elimination of Dirichlet rows and columns from a finite element stiffness matrix.

We close this section with a result which confirms well-posedness of the (square) system (3.27) and which will later serve to demonstrate well-posedness of our RB approximation.

**Lemma 3.1.** *There exists a constant  $C > 0$  such that the minimum eigenvalue of  $\mathbb{A}(\mu)$ ,  $\lambda_{\min}(\mu)$ , satisfies  $\lambda_{\min}(\mu) \geq C$ ,  $\forall \mu \in \mathcal{D}$ .*

*Proof.* From Lemma 3.1 in [7] we obtain,

$$a^o(\mathcal{W}(\mu^{\text{geo}})v, \mathcal{W}(\mu^{\text{geo}})v; \mu^{\text{coeff}}) \geq C_1(\Omega^o(\mu)) \sum_{p=1}^{n^\Gamma} (\mathcal{W}(\mu^{\text{geo}})v, \mathcal{W}(\mu^{\text{geo}})v)_{L^2(\Gamma_p^o(\mu^{\text{geo}}))}, \quad \forall v \in X_S^h(\mu), \quad (3.33)$$

**Algorithm 1.** Assembly of truth Schur complement system

---

```

1:  $\mathbb{F}(\mu) = 0, \mathbb{A}(\mu) = 0$ 
2: for  $i = 1, \dots, I$  do
3:   for  $j' = 1, \dots, n_{\mathcal{M}(i)}^\gamma$  do
4:     for  $k' = 1, \dots, \mathcal{N}_{\mathcal{M}(i),j'}^\gamma$  do
5:        $\mathbb{F}_{\mathcal{G}_i(j'),k'} += \mathbb{F}_{j',k'}^i(\mu_i)$ 
6:       for  $j = 1, \dots, n_{\mathcal{M}(i)}^\gamma$  do
7:         for  $k = 1, \dots, \mathcal{N}_{\mathcal{M}(i),j}^\gamma$  do
8:            $\mathbb{A}_{(\mathcal{G}_i(j'),k'),(\mathcal{G}_i(j),k)} += \mathbb{A}_{(j',k'),(j,k)}^i(\mu_i)$ 
9:         end for
10:      end for
11:    end for
12:  end for
13: end for

```

---

for  $C_1(\Omega^o(\mu)) > 0$ ; since  $\mathcal{D}$  is compact, we can further conclude that there exists  $C_2 > 0$  such that

$$a^o(\mathcal{W}(\mu^{\text{geo}})v, \mathcal{W}(\mu^{\text{geo}})v; \mu^{\text{coeff}}) \geq C_2 \sum_{p=1}^{n^\Gamma} (\mathcal{W}(\mu^{\text{geo}})v, \mathcal{W}(\mu^{\text{geo}})v)_{L^2(\Gamma_p^o(\mu^{\text{geo}}))}, \quad \forall v \in X_S^h(\mu), \quad \forall \mu \in \mathcal{D}. \quad (3.34)$$

We can rewrite (3.34) in terms of simpler notation as follows

$$a(v, v; \mu) \geq C_2(v, v)_{S^o}, \quad \forall v \in X_S^h(\mu), \quad \forall \mu \in \mathcal{D}, \quad (3.35)$$

recalling (3.22).

Next, for any  $v, w \in X_S^h(\mu)$  expressed in terms of the basis  $\{\Phi_{p,k}: 1 \leq p \leq n^\Gamma, 1 \leq k \leq \mathcal{N}_p^\Gamma\}$  with coefficient vectors  $\mathbb{V}, \mathbb{W} \in \mathbb{R}^{n_{\text{sc}}}$ , we obtain from (3.10)

$$(v, w)_{S^o} = \mathbb{W}^\top \mathbb{D}(\mu^{\text{geo}}) \mathbb{V}, \quad (3.36)$$

where  $\mathbb{D}(\mu^{\text{geo}}) \in \mathbb{R}^{n_{\text{sc}} \times n_{\text{sc}}}$  accounts for the effect of  $\mathcal{W}(\mu^{\text{geo}})$ . Note that we assume that  $\mathcal{W}(\mu^{\text{geo}})$  maps each reference port affinely, and hence  $\mathbb{D}(\mu^{\text{geo}})$  is diagonal since the orthogonality of our port modes from (3.10) is retained even though orthonormality is, in general, not preserved. Also, the diagonal entries of  $\mathbb{D}(\mu^{\text{geo}})$  are given by the determinant of the Jacobian of the port mappings, which from (2.7) are positive and bounded below by  $(\rho_{\text{LB}}^A)^{d-1}$ . Also, from (3.28)

$$a(v, w; \mu) = \mathbb{W}^\top \mathbb{A}(\mu) \mathbb{V}. \quad (3.37)$$

Hence, from (3.34), (3.36) and (3.37) we obtain the Rayleigh quotient lower bound,

$$\lambda_{\min}^o(\mu) \equiv \min_{\mathbb{V} \in \mathbb{R}^{n_{\text{sc}}}} \frac{\mathbb{V}^\top \mathbb{A}(\mu) \mathbb{V}}{\mathbb{V}^\top \mathbb{D}(\mu^{\text{geo}}) \mathbb{V}} = \min_{v \in X_S^h(\mu)} \frac{a(v, v; \mu)}{(v, v)_{S^o}} \geq C_2. \quad (3.38)$$

Finally, the result follows by noting that

$$\lambda_{\min}(\mu) \equiv \min_{\mathbb{V} \in \mathbb{R}^{n_{\text{sc}}}} \frac{\mathbb{V}^\top \mathbb{A}(\mu) \mathbb{V}}{\mathbb{V}^\top \mathbb{V}} \geq (\rho_{\text{LB}}^A)^{d-1} \min_{\mathbb{V} \in \mathbb{R}^{n_{\text{sc}}}} \frac{\mathbb{V}^\top \mathbb{A}(\mu) \mathbb{V}}{\mathbb{V}^\top \mathbb{D}(\mu^{\text{geo}}) \mathbb{V}} \geq C,$$

for  $C \equiv (\rho_{\text{LB}}^A)^{d-1} C_2$ . □

## 4. STATIC CONDENSATION REDUCED BASIS ELEMENT METHOD

The static condensation procedure described above is of course very computationally expensive due to the many “bubble solves” required on each component. However, we now introduce a Reduced Basis (RB) approximation: in particular, we follow exactly the same procedure as in Section 3.2, except now we introduce RB approximations for the bubble functions  $b_i^{f;h}(\mu_i)$ ,  $b_{i,j,k}^h(\mu_i)$ . As we shall demonstrate, the resulting numerical approach will offer considerable computational savings.

To begin, from (3.18), for each instantiated component we define the RB approximation  $\tilde{b}_i^f(\mu_i) \in \tilde{B}_{\mathcal{M}(i);0}^f$ ,

$$a_{\mathcal{M}(i)}(\tilde{b}_i^f(\mu_i), v; \mu_i) = f_{\mathcal{M}(i)}(v; \mu_i), \quad \forall v \in \tilde{B}_{\mathcal{M}(i);0}^f, \quad (4.1)$$

where the RB spaces  $\tilde{B}_{m;0}$  are constructed for each  $i = 1, \dots, M$  from the standard Greedy algorithm [27]. Note that there is one RB bubble approximation  $\tilde{b}_i^f(\mu_i)$  for each instantiated component. Next, from (3.19), we define the RB approximations  $\tilde{b}_{i,j,k}(\mu_i) \in \tilde{B}_{\mathcal{M}(i),j,k;0}$ ,

$$a_{\mathcal{M}(i)}(\tilde{b}_{i,j,k}(\mu_i), v; \mu_i) = -a_{\mathcal{M}(i)}(\psi_{\mathcal{M}(i),j,k}, v; \mu_i), \quad \forall v \in \tilde{B}_{\mathcal{M}(i),j,k;0}, \quad (4.2)$$

for  $1 \leq i \leq I$ ,  $1 \leq j \leq n_{\mathcal{M}(i)}^\gamma$ ,  $1 \leq k \leq \mathcal{N}_{\mathcal{M}(i),j}^\gamma$ . Here  $\tilde{B}_{m,j,k;0}$  is an RB approximation space – a *different* RB approximation space for each  $\{m, j, k\}$  – obtained by a standard Greedy [27] procedure.

The problems (4.1), (4.2) are well-posed due to our coercivity assumption. Note that thanks to our eigenfunction port representation the higher-mode (larger  $k$ ) bubble functions will typically vanish rapidly into the interior of the component – as seen in Figure 3 for example – and thus in many cases these higher modes will depend relatively weakly on the parameter. Therefore we expect that for most of the bubble degrees of freedom a *small* RB space will suffice.

Next, in analogy to (3.20), for  $1 \leq p \leq n^\Gamma$  and  $1 \leq k \leq \mathcal{N}_p^\Gamma$ , we define

$$\tilde{\Phi}_{p,k}(\mu) \equiv \Psi_{p,k} + \sum_{(i',j') \in \pi_p} \tilde{b}_{i',j',k}(\mu_{i'}) \mathbf{e}_{i'} = \sum_{(i',j') \in \pi_p} (\psi_{i',j',k} + \tilde{b}_{i',j',k}(\mu_{i'})) \mathbf{e}_{i'}, \quad (4.3)$$

and then

$$\tilde{X}_S(\mu) \equiv \text{span}\{\tilde{\Phi}_{p,k}(\mu) : 1 \leq p \leq n^\Gamma, 1 \leq k \leq \mathcal{N}_p^\Gamma\} \cap X^h. \quad (4.4)$$

We endow  $\tilde{X}_S(\mu)$  with the same inner product and norm as  $X_S^h(\mu)$ . From (3.25), (3.26) it is then natural to define  $\tilde{u}(\mu) \in \tilde{X}_S(\mu)$  as

$$\tilde{u}(\mu) \equiv \sum_{i=1}^I \tilde{b}_i^f(\mu_i) \mathbf{e}_i + \sum_{p=1}^{n^\Gamma} \sum_{k=1}^{\mathcal{N}_p^\Gamma} \tilde{U}_{p,k}(\mu) \tilde{\Phi}_{p,k}(\mu), \quad (4.5)$$

where the coefficients  $\tilde{U}_{p,k}(\mu)$  satisfy

$$\sum_{p=1}^{n^\Gamma} \sum_{k=1}^{\mathcal{N}_p^\Gamma} \tilde{U}_{p,k}(\mu) a(\tilde{\Phi}_{p,k}(\mu), v; \mu) = f(v; \mu) - \sum_{i=1}^I a(\tilde{b}_i^f(\mu_i) \mathbf{e}_i, v; \mu), \quad \forall v \in \tilde{X}_S(\mu). \quad (4.6)$$

We now identify the linear algebraic structure associated with (4.6).

In particular, we test in (4.6) on  $\tilde{\Phi}_{p',k'}(\mu)$  for  $1 \leq p' \leq n^\Gamma$ ,  $1 \leq k' \leq \mathcal{N}_{p'}^\Gamma$ , to obtain our “RB static condensation” system of dimension  $n_{sc}$ ,

$$\tilde{\mathbb{A}}(\mu) \tilde{\mathbb{U}}(\mu) = \tilde{\mathbb{F}}(\mu), \quad (4.7)$$

for the vector  $\tilde{\mathbb{U}}(\mu) \in \mathbb{R}^{n_{\text{sc}}}$  of coefficients  $\tilde{U}_{p,k}(\mu)$ . Note that the RB system (4.7) is the *same* size as the truth system (3.27): *a priori*, there is no reduction of the truth port degrees of freedom. Furthermore, our RBE system output can be expressed as

$$\tilde{s}(\mu) \equiv (\mathbb{L}^1(\mu) + \tilde{\mathbb{L}}^2(\mu))^T \tilde{\mathbb{U}}(\mu) + \sum_{i=1}^I \ell(\tilde{b}_i^f(\mu_i) \mathbf{e}_i; \mu). \quad (4.8)$$

We now define these RBE static condensation quantities more explicitly.

The matrix  $\tilde{\mathbb{A}}(\mu) \in \mathbb{R}^{n_{\text{sc}} \times n_{\text{sc}}}$  and vector  $\tilde{\mathbb{F}}(\mu) \in \mathbb{R}^{n_{\text{sc}}}$  are defined as

$$\tilde{\mathbb{A}}_{(p',k'),(p,k)}(\mu) \equiv a(\tilde{\Phi}_{p,k}(\mu), \tilde{\Phi}_{p',k'}(\mu); \mu), \quad (4.9)$$

and

$$\tilde{\mathbb{F}}_{p',k'}(\mu) \equiv f(\tilde{\Phi}_{p',k'}(\mu); \mu) - \sum_{i=1}^I a(\tilde{b}_i^f(\mu_i), \tilde{\Phi}_{p',k'}(\mu); \mu), \quad (4.10)$$

respectively, for  $1 \leq p \leq n^I$ ,  $1 \leq k \leq \mathcal{N}_p^I$ , and  $1 \leq p' \leq n^I$ ,  $1 \leq k' \leq \mathcal{N}_{p'}^I$ ; from (4.9) it is clear that  $\tilde{\mathbb{A}}(\mu)$  is symmetric. The output vector  $\mathbb{L}^1$  is defined in (3.30) and the output vector  $\tilde{\mathbb{L}}^2(\mu) \in \mathbb{R}^{n_{\text{sc}}}$  is given by

$$\tilde{\mathbb{L}}_{p,k}^2(\mu) \equiv \sum_{(i',j') \in \pi_p} \ell(\tilde{b}_{i',j',k}(\mu_{i'}) \mathbf{e}_{i'}), \quad (4.11)$$

for  $1 \leq p \leq n^I$ ,  $1 \leq k \leq \mathcal{N}_p^I$ .

We now introduce the reduced basis versions of the “local stiffness matrix” and “local load vector”: for each instantiated component, from (4.3)

$$\tilde{\mathbb{A}}_{(j',k'),(j,k)}^i(\mu_i) \equiv a_{\mathcal{M}(i)}(\psi_{\mathcal{M}(i),j,k} + \tilde{b}_{i,j,k}(\mu_i), \psi_{\mathcal{M}(i),j',k'} + \tilde{b}_{i,j',k'}(\mu_i); \mu), \quad (4.12)$$

$$\tilde{\mathbb{F}}_{j',k'}^i(\mu_i) \equiv f_{\mathcal{M}(i)}(\psi_{\mathcal{M}(i),j',k'} + \tilde{b}_{i,j',k'}(\mu_i); \mu_i) - a_{\mathcal{M}(i)}(\tilde{b}_i^f(\mu_i), \psi_{\mathcal{M}(i),j',k'} + \tilde{b}_{i,j',k'}(\mu_i); \mu_i), \quad (4.13)$$

for  $1 \leq j \leq n_{\mathcal{M}(i)}^\gamma$ ,  $1 \leq k \leq \mathcal{N}_{\mathcal{M}(i),j}^\gamma$ , and  $1 \leq j' \leq n_{\mathcal{M}(i)}^\gamma$ ,  $1 \leq k' \leq \mathcal{N}_{\mathcal{M}(i),j'}^\gamma$ . Algorithm 2 then defines the assembly procedure by which we construct (4.9), (4.10) from (4.12), (4.13). As in the truth case, Algorithm 2 requires minor post-processing in the case of Dirichlet boundary conditions.

---

**Algorithm 2.** Assembly of RB Schur complement system

---

- 1:  $\tilde{\mathbb{F}}(\mu) = 0$ ,  $\tilde{\mathbb{A}}(\mu) = 0$
  - 2: **for**  $i = 1, \dots, I$  **do**
  - 3:   **for**  $j' = 1, \dots, n_{\mathcal{M}(i)}^\gamma$  **do**
  - 4:     **for**  $k' = 1, \dots, \mathcal{N}_{\mathcal{M}(i),j'}^\gamma$  **do**
  - 5:        $\tilde{\mathbb{F}}_{\mathcal{G}_i(j'),k'}^i \ += \tilde{\mathbb{F}}_{j',k'}^i(\mu_i)$
  - 6:       **for**  $j = 1, \dots, n_{\mathcal{M}(i)}^\gamma$  **do**
  - 7:          **for**  $k = 1, \dots, \mathcal{N}_{\mathcal{M}(i),j}^\gamma$  **do**
  - 8:            $\tilde{\mathbb{A}}_{(\mathcal{G}_i(j'),k'),(\mathcal{G}_i(j),k)}^i \ += \tilde{\mathbb{A}}_{(j',k'),(j,k)}^i(\mu_i)$
  - 9:          **end for**
  - 10:       **end for**
  - 11:     **end for**
  - 12:   **end for**
  - 13: **end for**
-



We prove well-posedness of the discrete problem in:

**Proposition 4.1.** *If  $\|\mathbb{A}(\mu) - \tilde{\mathbb{A}}(\mu)\|_2 < \lambda_{\min}(\mu)$ , then  $\tilde{\lambda}_{\min}(\mu) > 0$ , where  $\tilde{\lambda}_{\min}(\mu)$  is the minimum eigenvalue of  $\tilde{\mathbb{A}}(\mu)$ . Also, we have*

$$\|\tilde{\mathbb{U}}(\mu)\|_2 \leq \frac{\sqrt{\gamma^{h,\text{cont}}(\mu)}}{\alpha^h(\mu)\sqrt{\lambda_{\min}(\mu) - \|\mathbb{A}(\mu) - \tilde{\mathbb{A}}(\mu)\|_2}} \|\hat{f}(\cdot; \mu)\|_{(X^h)',} \quad (4.14)$$

where  $\hat{f}(v; \mu) \equiv f(v; \mu) - \sum_{i=1}^I a(\tilde{b}_i^f(\mu_i) \mathbf{e}_i, v; \mu)$ , and

$$\|\hat{f}(\cdot; \mu)\|_{(X^h)'} \equiv \sup_{v \in X^h} \frac{\hat{f}(v; \mu)}{\|v\|_X}.$$

Here for  $v \in \mathbb{R}^n$  (respectively,  $A \in \mathbb{R}^{n \times n}$ ),  $\|\cdot\|_2$  refers to the Euclidean norm  $\|v\|_2 \equiv (v^T v)^{1/2}$  (respectively, induced norm  $\|A\|_2 \equiv \sup_{v \in \mathbb{R}^n} \|Av\|_2 / \|v\|_2$ ).

*Proof.* First we consider the bound for  $\tilde{\lambda}_{\min}(\mu)$ . We have

$$\begin{aligned} \tilde{\lambda}_{\min}(\mu) &= \min_{\mathbb{V} \in \mathbb{R}^{n_{\text{sc}}}} \frac{\mathbb{V}^T \tilde{\mathbb{A}}(\mu) \mathbb{V}}{\mathbb{V}^T \mathbb{V}} \\ &= \min_{\mathbb{V} \in \mathbb{R}^{n_{\text{sc}}}} \frac{\mathbb{V}^T (\mathbb{A}(\mu) + (\tilde{\mathbb{A}}(\mu) - \mathbb{A}(\mu))) \mathbb{V}}{\mathbb{V}^T \mathbb{V}} \\ &\leq \min_{\mathbb{V} \in \mathbb{R}^{n_{\text{sc}}}} \left( \frac{\mathbb{V}^T \mathbb{A}(\mu) \mathbb{V}}{\mathbb{V}^T \mathbb{V}} + \max_{\mathbb{W} \in \mathbb{R}^{n_{\text{sc}}}} \left| \frac{\mathbb{W}^T (\tilde{\mathbb{A}}(\mu) - \mathbb{A}(\mu)) \mathbb{W}}{\mathbb{W}^T \mathbb{W}} \right| \right) \\ &= \min_{\mathbb{V} \in \mathbb{R}^{n_{\text{sc}}}} \frac{\mathbb{V}^T \mathbb{A}(\mu) \mathbb{V}}{\mathbb{V}^T \mathbb{V}} + \max_{\mathbb{V} \in \mathbb{R}^{n_{\text{sc}}}} \left| \frac{\mathbb{V}^T (\tilde{\mathbb{A}}(\mu) - \mathbb{A}(\mu)) \mathbb{V}}{\mathbb{V}^T \mathbb{V}} \right| \end{aligned}$$

and thus

$$\tilde{\lambda}_{\min}(\mu) - \lambda_{\min}(\mu) \leq \max_{\mathbb{V} \in \mathbb{R}^{n_{\text{sc}}}} \left| \frac{\mathbb{V}^T (\tilde{\mathbb{A}}(\mu) - \mathbb{A}(\mu)) \mathbb{V}}{\mathbb{V}^T \mathbb{V}} \right|.$$

Exchanging the roles of  $\lambda_{\min}(\mu)$  and  $\tilde{\lambda}_{\min}(\mu)$  permits us to conclude that

$$|\lambda_{\min}(\mu) - \tilde{\lambda}_{\min}(\mu)| \leq \max_{\mathbb{V} \in \mathbb{R}^{n_{\text{sc}}}} \left| \frac{\mathbb{V}^T (\tilde{\mathbb{A}}(\mu) - \mathbb{A}(\mu)) \mathbb{V}}{\mathbb{V}^T \mathbb{V}} \right|.$$

We may then bound the right-hand side as

$$\begin{aligned} \max_{\mathbb{V} \in \mathbb{R}^{n_{\text{sc}}}} \left| \frac{\mathbb{V}^T (\mathbb{A}(\mu) - \tilde{\mathbb{A}}(\mu)) \mathbb{V}}{\mathbb{V}^T \mathbb{V}} \right| &\leq \max_{\mathbb{V} \in \mathbb{R}^{n_{\text{sc}}}} \frac{\|\mathbb{V}\|_2 \|(\mathbb{A}(\mu) - \tilde{\mathbb{A}}(\mu)) \mathbb{V}\|_2}{\|\mathbb{V}\|_2^2} \\ &= \max_{\mathbb{V} \in \mathbb{R}^{n_{\text{sc}}}} \frac{\|(\mathbb{A}(\mu) - \tilde{\mathbb{A}}(\mu)) \mathbb{V}\|_2}{\|\mathbb{V}\|_2} \\ &= \|\mathbb{A}(\mu) - \tilde{\mathbb{A}}(\mu)\|_2. \end{aligned}$$

Positivity of  $\tilde{\lambda}_{\min}(\mu)$  then follows from our hypothesis on  $\|\mathbb{A}(\mu) - \tilde{\mathbb{A}}(\mu)\|_2$  and the lower bound for  $\lambda_{\min}(\mu)$  in Lemma 3.1.

Next, we consider the bound for  $\|\tilde{\mathbb{U}}(\mu)\|_2$ . Let

$$\tilde{u}_{\mathcal{S}}(\mu) \equiv \sum_{p=1}^{n^r} \sum_{k=1}^{N_p^r} \tilde{U}_{p,k}(\mu) \tilde{\Phi}_{p,k}(\mu) \in \tilde{X}_{\mathcal{S}}(\mu).$$

Then from (4.6) we have

$$a(\tilde{u}_{\mathcal{S}}(\mu), v; \mu) = \hat{f}(v; \mu), \quad \forall v \in \tilde{X}_{\mathcal{S}}(\mu). \quad (4.15)$$

Since  $\tilde{X}_{\mathcal{S}}(\mu) \subset X^h$ , it follows from coercivity that

$$\alpha^h(\mu) \|\tilde{u}_{\mathcal{S}}(\mu)\|_X^2 \leq a(\tilde{u}_{\mathcal{S}}(\mu), \tilde{u}_{\mathcal{S}}(\mu); \mu) = \hat{f}(\tilde{u}_{\mathcal{S}}(\mu); \mu) \leq \|\hat{f}(\cdot; \mu)\|_{(X^h)'} \|\tilde{u}_{\mathcal{S}}(\mu)\|_X. \quad (4.16)$$

Hence, from (4.16) and continuity of  $a(\cdot, \cdot; \mu)$ , we have

$$(a(\tilde{u}_{\mathcal{S}}(\mu), \tilde{u}_{\mathcal{S}}(\mu); \mu))^{1/2} \leq \sqrt{\gamma^{h, \text{cont}}(\mu)} \|\tilde{u}_{\mathcal{S}}(\mu)\|_X \leq \frac{\sqrt{\gamma^{h, \text{cont}}(\mu)}}{\alpha^h(\mu)} \|\hat{f}(\cdot; \mu)\|_{(X^h)'}. \quad (4.17)$$

Next, we invoke the eigenvalue bound  $\tilde{\lambda}_{\min}(\mu) \geq \lambda_{\min}(\mu) - \|\mathbb{A}(\mu) - \tilde{\mathbb{A}}(\mu)\|_2$  from above to obtain

$$a(\tilde{u}_{\mathcal{S}}(\mu), \tilde{u}_{\mathcal{S}}(\mu); \mu) = \tilde{\mathbb{U}}(\mu)^T \tilde{\mathbb{A}}(\mu) \tilde{\mathbb{U}}(\mu) \geq (\lambda_{\min}(\mu) - \|\mathbb{A}(\mu) - \tilde{\mathbb{A}}(\mu)\|_2) \|\tilde{\mathbb{U}}(\mu)\|_2^2. \quad (4.18)$$

Finally, substitution of (4.18) into (4.17) yields the desired result. Note that  $\|\hat{f}(\cdot; \mu)\|_{(X^h)'}$  is finite thanks to boundedness of  $f$ , continuity of  $a$ , and well-posedness of (4.1).  $\square$

Proposition 4.1 implies that the static condensation RBE approximation is guaranteed to be well-posed in the limit that the errors in the RB bubble approximations tend to zero; the proposition furthermore establishes stability of the approximation. Further *a priori* results in particular related to convergence are difficult [5, 8] and we instead pass to computable *a posteriori* bounds. Note that the dual norm over  $(X^h)'$  is a global quantity that we will in fact eschew in our actual computational procedures (*e.g.*, for error bounds).

## 5. A POSTERIORI ERROR ANALYSIS

We now develop a bound for the error in the system level approximation. Our approach exploits standard RB *a posteriori* error estimators [28] at the component level to develop a bound for  $\|\mathbb{A}(\mu) - \tilde{\mathbb{A}}(\mu)\|_2$ ; we then apply matrix perturbation analysis [13] at the system level to arrive at an *a posteriori* bound for  $\|\mathbb{U}(\mu) - \tilde{\mathbb{U}}(\mu)\|_2$  and  $|s^h(\mu) - \tilde{s}(\mu)|$ .

### 5.1. Reduced basis preliminaries

For each  $1 \leq i \leq I$ ,  $1 \leq j \leq n_{\mathcal{M}(i)}^\gamma$ ,  $1 \leq k \leq N_{\mathcal{M}(i),j}^\gamma$ , the residual  $r_i^{f;h}(\cdot; \mu_i): B_{\mathcal{M}(i);0}^h \rightarrow \mathbb{R}$  for (4.1) is given by

$$r_i^{f;h}(v; \mu_i) \equiv f_{\mathcal{M}(i)}(v; \mu_i) - a_{\mathcal{M}(i)}(\tilde{b}_i^f(\mu_i), v; \mu_i), \quad \forall v \in B_{\mathcal{M}(i);0}^h; \quad (5.1)$$

similarly, the residual  $r_{i,j,k}^h(\cdot; \mu): B_{\mathcal{M}(i);0}^h \rightarrow \mathbb{R}$  for (4.2) is given by

$$r_{i,j,k}^h(v; \mu_i) \equiv -a_{\mathcal{M}(i)}(\psi_{\mathcal{M}(i),j,k} + \tilde{b}_{i,j,k}(\mu_i), v; \mu_i), \quad \forall v \in B_{\mathcal{M}(i);0}^h. \quad (5.2)$$

Let  $\mathcal{R}_i^f(\mu_i)$  (respectively,  $\mathcal{R}_{i,j,k}(\mu_i)$ ) denote the dual norm of the residual (5.1) (respectively, (5.2)),

$$\mathcal{R}_i^f(\mu_i) \equiv \sup_{v \in B_{\mathcal{M}(i);0}^h} \frac{r_i^{f;h}(v; \mu_i)}{\|v\|_{X_{\mathcal{M}(i)}}}, \quad (5.3)$$

$$\mathcal{R}_{i,j,k}(\mu_i) \equiv \sup_{v \in B_{\mathcal{M}(i);0}^h} \frac{r_{i,j,k}^h(v; \mu_i)}{\|v\|_{X_{\mathcal{M}(i)}}}. \quad (5.4)$$

Note the dual norms are defined with respect to the truth bubble spaces, as our static condensation RBE error is defined relative to the truth FE.

The *a posteriori* error bounds for the bubble approximations may then be expressed in terms of these residuals, as demonstrated in

**Lemma 5.1.** *For instantiated component  $i$  (where  $1 \leq i \leq I$ ), and  $\mu_i \in \hat{\mathcal{D}}_{\mathcal{M}(i)}$ , we have*

$$\|b_i^{f;h}(\mu_i) - \tilde{b}_i^f(\mu_i)\|_{X_{\mathcal{M}(i)}} \leq \frac{\mathcal{R}_i^f(\mu_i)}{\alpha_{\mathcal{M}(i);0}^{h,\text{LB}}(\mu_i)}, \quad (5.5)$$

$$\|b_{i,j,k}^h(\mu_i) - \tilde{b}_{i,j,k}(\mu_i)\|_{X_{\mathcal{M}(i)}} \leq \frac{\mathcal{R}_{i,j,k}(\mu_i)}{\alpha_{\mathcal{M}(i);0}^{h,\text{LB}}(\mu_i)}, \quad (5.6)$$

for  $1 \leq j \leq n_{\mathcal{M}(i)}^\gamma$ ,  $1 \leq k \leq \mathcal{N}_{\mathcal{M}(i),j}^\gamma$ . Here  $\alpha_{m;0}^{h,\text{LB}}(\hat{\mu}_m)$  satisfies

$$0 < \alpha_{m;0}^{h,\text{LB}}(\hat{\mu}_m) \leq \alpha_{m;0}^h(\hat{\mu}_m), \quad \forall \hat{\mu}_m \in \hat{\mathcal{D}}_m, \quad (5.7)$$

and  $\alpha_{m;0}^h(\hat{\mu}_m)$  is the coercivity constant from (3.2).

*Proof.* We refer to the RB literature for the proof of this standard result (e.g. [27, 28]).  $\square$

Note that, in actual practice, we evaluate  $\alpha_{m;0}^{h,\text{LB}}(\hat{\mu}_m)$  via the “min- $\Theta$ ” approach [28], or by the successive constraint method [18, 28].

## 5.2. System level bounds

We first derive bounds for the perturbation error in the statically condensed system matrix and load vector in

**Lemma 5.2.** *For any  $\mu \in \mathcal{D}$ ,  $\|\mathbb{F}(\mu) - \tilde{\mathbb{F}}(\mu)\|_2 \leq \sigma_1(\mu)$  and  $\|\mathbb{A}(\mu) - \tilde{\mathbb{A}}(\mu)\|_F \leq \sigma_2(\mu)$ . Here  $\|\cdot\|_F$  denotes the matrix Frobenius norm and*

$$\sigma_1(\mu) \equiv \left\{ 2 \sum_{i=1}^I \left( \Delta_i^f(\mu_i) \right)^2 \left( \sum_{j=1}^{n_{\mathcal{M}(i)}^\gamma} \sum_{k=1}^{\mathcal{N}_{\mathcal{M}(i),j}^\gamma} (\Delta_{i,j,k}(\mu_i))^2 \right) \right\}^{1/2}, \quad (5.8)$$

$$\sigma_2(\mu) \equiv \left\{ 2 \sum_{i=1}^I \left( \sum_{j=1}^{n_{\mathcal{M}(i)}^\gamma} \sum_{k=1}^{\mathcal{N}_{\mathcal{M}(i),j}^\gamma} (\Delta_{i,j,k}(\mu_i))^2 \right) \right\}^{1/2}, \quad (5.9)$$

where

$$\Delta_i^f(\mu_i) \equiv \mathcal{R}_i^f(\mu_i) / \sqrt{\alpha_{\mathcal{M}(i);0}^{h,\text{LB}}(\mu_i)}, \quad (5.10)$$

$$\Delta_{i,j,k}(\mu_i) \equiv \mathcal{R}_{i,j,k}(\mu_i) / \sqrt{\alpha_{\mathcal{M}(i);0}^{h,\text{LB}}(\mu_i)}, \quad (5.11)$$

for  $\alpha_{m;0}^{h,\text{LB}}(\cdot)$  satisfying (5.7).

*Proof.* The proofs for (5.8) and (5.9) are similar and we thus restrict attention to the more involved case, (5.9). To derive a bound for  $\|\mathbb{A}(\mu) - \tilde{\mathbb{A}}(\mu)\|_F$ , we start with a component-level bound for  $\|\mathbb{A}^i(\mu) - \tilde{\mathbb{A}}^i(\mu)\|_F$ . For the error in a single entry on instantiated component  $i$ , we have

$$\begin{aligned} & \left| \mathbb{A}_{(j',k'),(j,k)}^i(\mu_i) - \tilde{\mathbb{A}}_{(j',k'),(j,k)}^i(\mu_i) \right| \\ &= \left| a_{\mathcal{M}(i)}(\psi_{\mathcal{M}(i),j,k}(\mu_i) + b_{i,j,k}^h(\mu_i), \psi_{\mathcal{M}(i),j',k'}(\mu_i); \mu_i) + b_{i,j',k'}^h(\mu_i); \mu_i) \right. \\ & \quad \left. - a_{\mathcal{M}(i)}(\psi_{\mathcal{M}(i),j,k}(\mu_i) + \tilde{b}_{i,j,k}(\mu_i), \psi_{\mathcal{M}(i),j',k'}(\mu_i); \mu_i) + \tilde{b}_{i,j',k'}(\mu_i); \mu_i) \right| \\ &= \left| a_{\mathcal{M}(i)}(b_{i,j,k}^h(\mu_i), \psi_{\mathcal{M}(i),j',k'}(\mu_i); \mu_i) + a_{\mathcal{M}(i)}(\psi_{\mathcal{M}(i),j,k}(\mu_i) + b_{i,j,k}^h(\mu_i), b_{i,j',k'}^h(\mu_i); \mu_i) \right. \\ & \quad \left. - a_{\mathcal{M}(i)}(\tilde{b}_{i,j,k}(\mu_i), \psi_{\mathcal{M}(i),j',k'}(\mu_i); \mu_i) - a_{\mathcal{M}(i)}(\psi_{\mathcal{M}(i),j,k}(\mu_i) + \tilde{b}_{i,j,k}(\mu_i), \tilde{b}_{i,j',k'}(\mu_i); \mu_i) \right|. \end{aligned} \quad (5.12)$$

Since  $b_{i,j',k'}^h(\mu_i) \in B_{\mathcal{M}(i);0}^h$ , it follows from (3.19) that

$$a_{\mathcal{M}(i)}(\psi_{\mathcal{M}(i),j,k}(\mu_i) + b_{i,j,k}^h(\mu_i), b_{i,j',k'}^h(\mu_i); \mu_i) = 0. \quad (5.13)$$

Also, from (3.19) and symmetry of  $a$ , we have

$$\begin{aligned} a_{\mathcal{M}(i)}(b_{i,j,k}^h(\mu_i), \psi_{\mathcal{M}(i),j',k'}(\mu_i); \mu_i) &= -a_{\mathcal{M}(i)}(b_{i,j,k}^h(\mu_i), b_{i,j',k'}^h(\mu_i); \mu_i) \\ &= a_{\mathcal{M}(i)}(\psi_{\mathcal{M}(i),j,k}(\mu_i), \tilde{b}_{i,j',k'}^h(\mu_i); \mu_i), \end{aligned} \quad (5.14)$$

and

$$a_{\mathcal{M}(i)}(\tilde{b}_{i,j,k}(\mu_i), \psi_{\mathcal{M}(i),j',k'}(\mu_i); \mu_i) = -a_{\mathcal{M}(i)}(\tilde{b}_{i,j,k}(\mu_i), b_{i,j',k'}^h(\mu_i); \mu_i). \quad (5.15)$$

Hence, (5.12) with (5.2), (5.13)–(5.15) implies

$$\begin{aligned} & \left| \mathbb{A}_{(j',k'),(j,k)}^i(\mu_i) - \tilde{\mathbb{A}}_{(j',k'),(j,k)}^i(\mu_i) \right| \\ &= \left| a_{\mathcal{M}(i)}(\psi_{\mathcal{M}(i),j,k}(\mu_i) + \tilde{b}_{i,j,k}(\mu_i), b_{i,j',k'}^h(\mu_i); \mu_i) \right. \\ & \quad \left. - a_{\mathcal{M}(i)}(\psi_{\mathcal{M}(i),j,k}(\mu_i) + \tilde{b}_{i,j,k}(\mu_i), \tilde{b}_{i,j',k'}(\mu_i); \mu_i) \right| \\ &= \left| a_{\mathcal{M}(i)}(\psi_{\mathcal{M}(i),j,k}(\mu_i) + \tilde{b}_{i,j,k}(\mu_i), b_{i,j',k'}^h(\mu_i) - \tilde{b}_{i,j',k'}(\mu_i); \mu_i) \right| \\ &= \left| r_{i,j,k}^h(b_{i,j',k'}^h(\mu_i) - \tilde{b}_{i,j',k'}(\mu_i); \mu_i) \right|. \end{aligned}$$

It thus follows from (5.4) and Lemma 5.1 that

$$\begin{aligned}
 & \left| \mathbb{A}_{(j',k'),(j,k)}^i(\mu_i) - \tilde{\mathbb{A}}_{(j',k'),(j,k)}^i(\mu_i) \right| \\
 &= \frac{\left| r_{i,j,k}^h(b_{i,j',k'}^h(\mu_i) - \tilde{b}_{i,j',k'}^h(\mu_i); \mu_i) \right|}{\left\| b_{i,j',k'}^h(\mu_i) - \tilde{b}_{i,j',k'}^h(\mu_i) \right\|_{X_{\mathcal{M}(i)}}} \left\| b_{i,j',k'}^h(\mu_i) - \tilde{b}_{i,j',k'}^h(\mu_i) \right\|_{X_{\mathcal{M}(i)}} \\
 &\leq \mathcal{R}_{i,j,k}(\mu_i) \left\| b_{i,j',k'}^h(\mu_i) - \tilde{b}_{i,j',k'}^h(\mu_i) \right\|_{X_{\mathcal{M}(i)}} \\
 &\leq \mathcal{R}_{i,j,k}(\mu_i) \mathcal{R}_{i,j',k'}(\mu_i) / \alpha_{\mathcal{M}(i);0}^{h,\text{LB}}(\mu_i) \\
 &= \Delta_{i,j,k}(\mu_i) \Delta_{i,j',k'}(\mu_i). \tag{5.16}
 \end{aligned}$$

Then, a Frobenius norm bound for the error in the “local stiffness matrix” for instantiated component  $i$  is given by

$$\begin{aligned}
 \left\| \mathbb{A}^i(\mu_i) - \tilde{\mathbb{A}}^i(\mu_i) \right\|_F^2 &\leq \sum_{j=1}^{n_{\mathcal{M}(i)}^\gamma} \sum_{k=1}^{\mathcal{N}_{\mathcal{M}(i),j}^\gamma} \sum_{j'=1}^{n_{\mathcal{M}(i)}^\gamma} \sum_{k'=1}^{\mathcal{N}_{\mathcal{M}(i),j'}^\gamma} (\Delta_{i,j,k}(\mu_i) \Delta_{i,j',k'}(\mu_i))^2 \\
 &= \left( \sum_{j=1}^{n_{\mathcal{M}(i)}^\gamma} \sum_{k=1}^{\mathcal{N}_{\mathcal{M}(i),j}^\gamma} \Delta_{i,j,k}(\mu_i)^2 \right) \left( \sum_{j'=1}^{n_{\mathcal{M}(i)}^\gamma} \sum_{k'=1}^{\mathcal{N}_{\mathcal{M}(i),j'}^\gamma} \Delta_{i,j',k'}(\mu_i)^2 \right) \\
 &= \left( \sum_{j=1}^{n_{\mathcal{M}(i)}^\gamma} \sum_{k=1}^{\mathcal{N}_{\mathcal{M}(i),j}^\gamma} \Delta_{i,j,k}(\mu_i)^2 \right)^2. \tag{5.17}
 \end{aligned}$$

Finally, we recall that we suppose that each entry of  $\mathbb{A}(\mu)$  and  $\tilde{\mathbb{A}}(\mu)$  is assembled from a sum of terms from at most two different local stiffness matrices; thus (5.9) follows from (5.17) and the inequality  $(a+b)^2 \leq 2(a^2+b^2)$ .  $\square$

We note that the proof of Lemma 5.2 relies on the symmetry of the  $a(\cdot, \cdot; \mu)$ ; the proof can be generalized to the non-symmetric case with a primal-dual RB formulation [28].

We now bound the solution error in

**Proposition 5.3.** *If  $\tilde{\lambda}_{\min}(\mu) > \sigma_2(\mu)$ , then*

$$\left\| \mathbb{U}(\mu) - \tilde{\mathbb{U}}(\mu) \right\|_2 \leq \Delta^{\mathbb{U}}(\mu), \tag{5.18}$$

where

$$\Delta^{\mathbb{U}}(\mu) \equiv \frac{\sigma_1(\mu) + \sigma_2(\mu) \left\| \tilde{\mathbb{U}}(\mu) \right\|_2 + \left\| \tilde{\mathbb{F}}(\mu) - \tilde{\mathbb{A}}(\mu) \tilde{\mathbb{U}}(\mu) \right\|_2}{\tilde{\lambda}_{\min}(\mu) - \sigma_2(\mu)}. \tag{5.19}$$

Recall that  $\|\cdot\|_2$  refers to the Euclidean norm.

*Proof.* Let  $\delta\mathbb{A}(\mu) \equiv \mathbb{A}(\mu) - \tilde{\mathbb{A}}(\mu)$ ,  $\delta\mathbb{F}(\mu) \equiv \mathbb{F}(\mu) - \tilde{\mathbb{F}}(\mu)$ , and  $\delta\mathbb{U}(\mu) = \mathbb{U}(\mu) - \tilde{\mathbb{U}}(\mu)$ . Then, from (3.27), we have the identity

$$[\tilde{\mathbb{A}}(\mu) + \delta\mathbb{A}(\mu)] \delta\mathbb{U}(\mu) = \delta\mathbb{F}(\mu) - \delta\mathbb{A}(\mu) \tilde{\mathbb{U}}(\mu) + (\tilde{\mathbb{F}}(\mu) - \tilde{\mathbb{A}}(\mu) \tilde{\mathbb{U}}(\mu)). \tag{5.20}$$

(Note if (4.7) is solved exactly then the last term on the right-hand side of (5.20) vanishes; however, we retain the term to accommodate (for example) iterative solution error). We pre-multiply (5.20) by  $\delta\mathbb{U}(\mu)^{\text{T}}$

and divide by  $\delta\mathbb{U}(\mu)^T \delta\mathbb{U}(\mu)$  to obtain

$$\begin{aligned} \tilde{\lambda}_{\min}(\mu) &\leq \frac{\delta\mathbb{U}(\mu)^T \tilde{\mathbb{A}}(\mu) \delta\mathbb{U}(\mu)}{\delta\mathbb{U}(\mu)^T \delta\mathbb{U}(\mu)} \leq \left| \frac{\delta\mathbb{U}(\mu)^T \delta\mathbb{F}(\mu)}{\delta\mathbb{U}(\mu)^T \delta\mathbb{U}(\mu)} \right| + \left| \frac{\delta\mathbb{U}(\mu)^T \delta\mathbb{A}(\mu) \tilde{\mathbb{U}}(\mu)}{\delta\mathbb{U}(\mu)^T \delta\mathbb{U}(\mu)} \right| \\ &\quad + \left| \frac{\delta\mathbb{U}(\mu)^T \delta\mathbb{A}(\mu) \delta\mathbb{U}(\mu)}{\delta\mathbb{U}(\mu)^T \delta\mathbb{U}(\mu)} \right| + \left| \frac{\delta\mathbb{U}(\mu)^T (\tilde{\mathbb{F}}(\mu) - \tilde{\mathbb{A}}(\mu) \tilde{\mathbb{U}}(\mu))}{\delta\mathbb{U}(\mu)^T \delta\mathbb{U}(\mu)} \right| \\ &\leq \frac{\|\delta\mathbb{F}(\mu)\|_2 + \|\delta\mathbb{A}(\mu) \tilde{\mathbb{U}}(\mu)\|_2 + \|\tilde{\mathbb{F}}(\mu) - \tilde{\mathbb{A}}(\mu) \tilde{\mathbb{U}}(\mu)\|_2}{\|\delta\mathbb{U}(\mu)\|_2} + \|\delta\mathbb{A}(\mu)\|_2 \quad (5.21) \end{aligned}$$

$$\begin{aligned} &\leq \frac{\|\delta\mathbb{F}(\mu)\|_2 + \|\delta\mathbb{A}(\mu)\|_2 \|\tilde{\mathbb{U}}(\mu)\|_2 + \|\tilde{\mathbb{F}}(\mu) - \tilde{\mathbb{A}}(\mu) \tilde{\mathbb{U}}(\mu)\|_2}{\|\delta\mathbb{U}(\mu)\|_2} + \|\delta\mathbb{A}(\mu)\|_2 \\ &\leq \frac{\sigma_1(\mu) + \sigma_2(\mu) \|\tilde{\mathbb{U}}(\mu)\|_2 + \|\tilde{\mathbb{F}}(\mu) - \tilde{\mathbb{A}}(\mu) \tilde{\mathbb{U}}(\mu)\|_2}{\|\delta\mathbb{U}(\mu)\|_2} + \sigma_2(\mu), \quad (5.22) \end{aligned}$$

where we have employed the bound  $\|\delta\mathbb{A}(\mu)\|_2 \leq \|\delta\mathbb{A}(\mu)\|_F \leq \sigma_2(\mu)$  (recall that  $\|\cdot\|_2 \leq \|\cdot\|_F$  is a consequence of the Cauchy–Schwarz inequality). The desired result (5.18), (5.19) then follows straightforwardly from (5.22).  $\square$

It is a consequence of Proposition 5.3 that as our RB bubble approximations converge then the system level RBE approximation also converges:

**Corollary 5.4.** *If  $\tilde{\mathbb{U}}(\mu) = \tilde{\mathbb{A}}(\mu)^{-1} \tilde{\mathbb{F}}(\mu)$  (i.e. the RB Schur complement system is solved exactly) and  $\sigma_1(\mu) \rightarrow 0$ ,  $\sigma_2(\mu) \rightarrow 0$ , then  $\Delta^{\mathbb{U}}(\mu) \rightarrow 0$ .*

*Proof.* The result directly follows from Proposition 4.1.  $\square$

Note we do not yet have bounds for the effectivity of our system level error estimator  $\Delta^{\mathbb{U}}(\mu)$ .

In this paper we shall primarily invoke the error bound of Proposition 5.3 in particular since the different contributions to the error bound (5.19) are readily identified. However, it is possible to develop a sharper bound as demonstrated in

**Corollary 5.5.** *If  $\tilde{\lambda}_{\min}(\mu) > \sigma_2(\mu)$ ,*

$$\|\mathbb{U}(\mu) - \tilde{\mathbb{U}}(\mu)\|_2 \leq \Delta_*^{\mathbb{U}}(\mu), \quad (5.23)$$

where

$$\Delta_*^{\mathbb{U}}(\mu) \equiv \frac{\sigma_1(\mu) + \sigma_3(\mu) + \|\tilde{\mathbb{F}}(\mu) - \tilde{\mathbb{A}}(\mu) \tilde{\mathbb{U}}(\mu)\|_2}{\tilde{\lambda}_{\min}(\mu) - \sigma_2(\mu)}, \quad (5.24)$$

and

$$\sigma_3(\mu) \equiv \left\{ 2 \sum_{i=1}^I \left( \sum_{j=1}^{n_{\mathcal{M}(i)}^{\gamma}} \sum_{k=1}^{\mathcal{N}_{\mathcal{M}(i),j}^{\gamma}} (\Delta_{i,j,k}(\mu_i))^2 \right) \left( \sum_{j=1}^{n_{\mathcal{M}(i)}^{\gamma}} \sum_{k=1}^{\mathcal{N}_{\mathcal{M}(i),j}^{\gamma}} \Delta_{i,j,k}(\mu_i) |\tilde{U}_{j,k}^i(\mu)| \right)^2 \right\}^{1/2}. \quad (5.25)$$

Note for instantiated component  $i$ ,  $\tilde{\mathbb{U}}^i \in \mathbb{R}^{\mathcal{N}_{\mathcal{M}(i)}^{\text{ports}}}$  is the subvector of  $\tilde{\mathbb{U}} \in \mathbb{R}^{n_{\text{sc}}}$  with entries  $\tilde{U}_{j,k}^i = \tilde{U}_{\mathcal{G}_i(j),k}$ ,  $1 \leq j \leq n_{\mathcal{M}(i)}^{\gamma}$ ,  $1 \leq k \leq \mathcal{N}_{\mathcal{M}(i),j}^{\gamma}$ .

*Proof.* We first develop a (sharper) bound for

$$\left| \frac{\delta\mathbb{U}(\mu)^T \delta\mathbb{A}(\mu) \tilde{\mathbb{U}}(\mu)}{\delta\mathbb{U}(\mu)^T \delta\mathbb{U}(\mu)} \right|. \quad (5.26)$$

To begin we invoke (5.16) to develop a bound for a single entry of the contribution from instantiated component  $i$ ,  $(\mathbb{A}^i - \tilde{\mathbb{A}}^i) \tilde{\mathbb{U}}^i$ , to the vector  $\delta\mathbb{A}(\mu) \tilde{\mathbb{U}}(\mu)$

$$\left| \sum_{j=1}^{n_{\mathcal{M}(i)}^\gamma} \sum_{k=1}^{\mathcal{N}_{\mathcal{M}(i),j}^\gamma} (\mathbb{A}_{(j',k'),(j,k)}^i(\mu_i) - \tilde{\mathbb{A}}_{(j',k'),(j,k)}^i(\mu_i)) \tilde{U}_{j,k}^i(\mu) \right| \leq \Delta_{i,j',k'}(\mu_i) \sum_{j=1}^{n_{\mathcal{M}(i)}^\gamma} \sum_{k=1}^{\mathcal{N}_{\mathcal{M}(i),j}^\gamma} \Delta_{i,j,k}(\mu_i) |\tilde{U}_{j,k}^i(\mu)|. \quad (5.27)$$

It thus follows from (5.27) that

$$\begin{aligned} \|(\mathbb{A}^i(\mu_i) - \tilde{\mathbb{A}}^i(\mu_i)) \tilde{\mathbb{U}}^i(\mu)\|_2^2 &\leq \sum_{j'=1}^{n_{\mathcal{M}(i)}^\gamma} \sum_{k'=1}^{\mathcal{N}_{\mathcal{M}(i),j'}^\gamma} \left( \Delta_{(i,j',k')}(\mu_i) \sum_{j=1}^{n_{\mathcal{M}(i)}^\gamma} \sum_{k=1}^{\mathcal{N}_{\mathcal{M}(i),j}^\gamma} \Delta_{i,j,k}(\mu_i) |\tilde{U}_{j,k}^i(\mu)| \right)^2 \\ &= \left( \sum_{j=1}^{n_{\mathcal{M}(i)}^\gamma} \sum_{k=1}^{\mathcal{N}_{\mathcal{M}(i),j}^\gamma} \Delta_{i,j,k}(\mu_i)^2 \right) \left( \sum_{j=1}^{n_{\mathcal{M}(i)}^\gamma} \sum_{k=1}^{\mathcal{N}_{\mathcal{M}(i),j}^\gamma} \Delta_{i,j,k}(\mu_i) |\tilde{U}_{j,k}^i(\mu)| \right)^2. \end{aligned} \quad (5.28)$$

We now recall the assumption that a component has at most one neighbor per port; hence, with the inequality  $(a+b)^2 \leq 2(a^2+b^2)$ , we can accumulate (5.28) over all  $i = 1, \dots, I$  to obtain

$$\|\delta\mathbb{A}(\mu) \tilde{\mathbb{U}}(\mu)\|_2 \leq \sigma_3(\mu). \quad (5.29)$$

The result then follows from (5.21) and (5.29).  $\square$

We anticipate that  $|\tilde{U}_{j,k}^i|$  will decrease (potentially quite rapidly) with  $k$ , and thus we can expect  $\Delta_*^\mathbb{U}(\mu) \ll \Delta^\mathbb{U}(\mu)$ . As  $\Delta_*^\mathbb{U}(\mu)$  and  $\Delta^\mathbb{U}(\mu)$  can be calculated at roughly the same cost, clearly  $\Delta_*^\mathbb{U}(\mu)$  is preferred in actual computational practice.

We close this section with error analysis for the system output. An *a posteriori* error bound for the system output  $\tilde{s}(\mu)$  is given in

**Proposition 5.6.** *Suppose that for all  $\mu \in \mathcal{D}$ ,  $\ell(\cdot, \mu): X^h \rightarrow \mathbb{R}$  satisfies*

$$\ell(v; \mu) = 0, \quad \forall v \in \bigoplus_{i=1}^I B_{\mathcal{M}(i);0}^h. \quad (5.30)$$

Then

$$|s^h(\mu) - \tilde{s}(\mu)| \leq \Delta^s(\mu), \quad (5.31)$$

for

$$\Delta^s(\mu) \equiv \Delta^\mathbb{U}(\mu) \|\mathbb{L}^1(\mu)\|_2 \quad (5.32)$$

(and similarly,  $|s^h(\mu) - \tilde{s}(\mu)| \leq \Delta_*^\mathbb{U}(\mu) \|\mathbb{L}^1(\mu)\|_2 \equiv \Delta_*^s(\mu)$ ).

*Proof.* From (3.14), (4.3), (4.5), (5.30), and the Cauchy–Schwarz inequality, we have

$$\begin{aligned} |s^h(\mu) - \tilde{s}(\mu)| &= |\ell(u^h(\mu) - \tilde{u}(\mu); \mu)| = \left| \sum_{p=1}^{n^\Gamma} \sum_{k=1}^{\mathcal{N}_p^\Gamma} (U_{p,k}(\mu) - \tilde{U}_{p,k}(\mu)) \ell(\Psi_{p,k}; \mu) \right| \\ &\leq \left( \sum_{p=1}^{n^\Gamma} \sum_{k=1}^{\mathcal{N}_p^\Gamma} (U_{p,k}(\mu) - \tilde{U}_{p,k}(\mu))^2 \right)^{1/2} \left( \sum_{p=1}^{n^\Gamma} \sum_{k=1}^{\mathcal{N}_p^\Gamma} \ell(\Psi_{p,k}; \mu)^2 \right)^{1/2} \\ &\leq \Delta^\mathbb{U}(\mu) \left( \sum_{p=1}^{n^\Gamma} \sum_{k=1}^{\mathcal{N}_p^\Gamma} \ell(\Psi_{p,k}; \mu)^2 \right)^{1/2}. \end{aligned}$$

The result then follows from the definition of  $\mathbb{L}^1(\mu)$  in (3.30).  $\square$

We note that outputs that satisfy (5.30) are common in applications and in particular many outputs are defined only over component ports. In fact, arguably the most common outputs of interest are defined by average quantities over ports, in which case all but a few terms in the sum  $\sum_{p=1}^{n^r} \sum_{k=1}^{N_p^r} \ell(\Psi_{p,k}; \mu)^2$  will vanish. It is straightforward (but somewhat cumbersome) to extend Proposition 5.6 to the general case in which  $\ell$  does not vanish over the bubble spaces and hence (5.30) is not satisfied. We omit this extension here since all of the outputs we consider in Section 7 do indeed satisfy (5.30).

A system level error bound is derived for the classical RBE method of Maday and Rønquist in [24]. A key difference between the result in [24] and Proposition 5.3 is that in our static condensation formulation we do not require component level truth calculations to estimate interface correction terms since our approximation is globally conforming.

## 6. COMPUTATIONAL PROCEDURES

### 6.1. Overview

The computations proceed in two stages: Offline and Online. These two stages are connected through an Online Dataset which is constructed in the Offline stage and then invoked in the Online stage. The Offline stage is performed once for any given library of archetype components; the Online stage is then performed many times for each new system (composed of instantiated elements from the library) or each new set of parameter values. The Offline stage is very expensive, whereas the Online stage is very inexpensive. Thus, as is always the case in the model order reduction paradigm, we focus on the real-time/interactive and many-query contexts in which the Offline stage investment is either irrelevant (*e.g.*, given a real-time imperative, as in parameter estimation) or amortized over many Online evaluations (*e.g.*, given a many-query requirement, as in design).

In the Offline stage we construct the bubble spaces  $\tilde{B}_{m,0}^f$  and  $\tilde{B}_{m,j,k;0}$  from (4.1) and (4.2), respectively, associated with the archetype components which comprise our library. We then generate the affine decomposition for the reduced basis archetype component stiffness matrices and the affine decomposition for the reduced basis error bound inner products to form the Online Dataset; note that the affine decomposition follows “standard” reduced basis practice [28]. In the Online stage we compute the reduced basis bubble approximations, evaluate the reduced basis Schur complement entries, solve the (reduced basis approximate) Schur system, compute the stability eigenvalue  $\tilde{\lambda}_{\min}$ , and finally evaluate the reduced basis and system error bounds. We shall address each of these steps in further detail below.

In contrast to the standard reduced basis method, RBE methods (our static condensation approach, as well as the classical RBE methods) consider many small reduced basis models each with only relatively few parameters rather than one reduced basis model with many parameters; we thus mitigate the curse of dimensionality as regards the number of parameters which may be feasibly treated. Furthermore, in RBE approaches we may consider *many* different systems and indeed different topologies and hence we may amortize or justify the Offline cost over many more Online appeals. Our static condensation RBE method offers further advantages relative to the classical RBE method: we can treat components as completely interoperable without reference to any generation configuration, and we may thus consider for any given Offline library a much wider class of Online systems. However, the increased flexibility afforded by the “configuration agnostic” static condensation RBE library does come at some computational cost in particular related to the many bubble functions associated with each component.

We discuss in this section the operation counts associated with the Offline and Online stages, respectively. We also propose some metrics for comparison of the computational cost of the static condensation RBE approach relative to the computational cost of more standard finite element approaches. In Section 7 we apply our framework for computational cost analysis to several numerical examples; in particular, we provide computational timings which justify our claims. Note we report all timings for an effective platform (an AMD Opteron 2382) though in some cases actual timings are performed on different machines and then translated to our common reference.



Before embarking we recall some notation and introduce some additional notation that will figure prominently in what follows. We recall that  $M$  denotes the number of archetype components in our library, and that  $I$  refers to the number of instantiated components in a particular system. In our formulation we obtain considerable savings in the case that we have “component repetition”. With this in mind, we introduce the concept of *component clones*: two instantiated components are clones if they share the same archetype component parent *and* the same parameter values. In fact, as regards the latter condition, for two components to be clones they need share only the same *non-docking* parameter values; recall that docking parameters are parameters which may affect the geometric configuration of the instantiated component but do not affect the bilinear form (*e.g.*, translation or rotation for a homogeneous and isotropic bilinear form). We let  $I'_{cs}$  denote the number of “clone sets”, where each clone set is the equivalence class of instantiated component clones.

Also, we note that the static condensation RBE formulation fits naturally within an iterative design process in which a sequence of simulations are performed with parameters or component connectivity varied from one iteration to the next. Within this context, the relevant “component repetition” concept is not the number of clone sets, but rather the number of clone sets in which the parameter values are varied relative to an immediately preceding Online evaluation – we define  $I'_{var}$  to be the number of “varied clone sets.” (Note that of course a given instantiated component need not remain in the same clone set from one design iteration to the next). We also highlight an important special case in which all component parameters remain the same but the component connectivity is modified in some way – we refer to this as a *rearrangement* of the system. In the case of a rearrangement we obtain  $I'_{var} = 0$ .

We recall that  $Q_{max}$  refers to the maximum number of terms in the affine sums over all affine decompositions over all archetype components in our library. We further define  $N_{max}$  to be the largest reduced basis bubble space dimension over all bubbles over all archetype components in our library. We recall that  $n_{sc}$  is the size of our Schur complement system, which in turn is bounded by the product of  $n^I$  and  $\mathcal{N}_{max}^I$ ; here  $n^I$  is the number of global ports in a system, and  $\mathcal{N}_{max}^I$  is the maximum number of (truth) degrees of freedom on a global port over all global ports. Finally, it shall be convenient to introduce  $\mathcal{N}_{max}^{ports}$  as the maximum number of port degrees of freedom in a component over all components; note that the number of port degrees of freedom in a component is the sum over the local ports of the number of (truth) degrees of freedom over each port.

## 6.2. Offline stage and online dataset

The Offline operation count has two main contributions. The *first contribution* combines the Greedy development of the bubble spaces (4.1), (4.2) with the associated formation of the reduced basis approximation and error bound affine decompositions [28]. It can be shown that this operation count scales roughly as

$$M\mathcal{N}_{max}^{ports}n_{train}(Q_{max}N_{max}^3 + Q_{max}^2N_{max}^3 + N_{max}^4) + MN_{max}\mathcal{F}^{FE}(\mathcal{N}_{max}^{com}) \quad (6.1)$$

where  $\mathcal{N}_{max}^{com}$  denotes the maximum number of truth FE degrees of freedom in a component over all components in a system,  $\mathcal{F}^{FE}(\mathcal{N})$  denotes the operation count to solve a sparse finite element discrete system of size  $\mathcal{N}$ , and  $n_{train}$  is the number of parameter points in the Greedy training set. The *second contribution* reflects the affine decomposition of the reduced basis Schur complement entries, which we may view as (multiple) outputs. It can be shown that this operation count scales roughly as

$$M(\mathcal{N}_{max}^{ports})^2Q_{max}N_{max}^2. \quad (6.2)$$

Note that in general in all of our operation counts (and memory estimates) we will neglect the cost associated with the bubbles associated with the inhomogeneity  $f$  – one per component – compared to the cost associated with the (many more) bubble functions associated with the port degrees of freedom.

The storage (memory) for the Online Dataset comprises two similar components. The storage associated with the affine decomposition of the reduced basis bubble approximations and associated error bounds is given roughly by  $M\mathcal{N}_{max}^{ports}(Q_{max}N_{max}^2 + Q_{max}^2N_{max}^2)$ ; note that the Greedy training set is only required in the Offline stage, not the Online stage, and hence the Online Dataset memory does not scale with (or indeed, depend on)  $n_{train}$ . The

storage associated with the reduced basis Schur complement entries is given roughly by  $M(\mathcal{N}_{\max}^{\text{ports}})^2 Q_{\max} N_{\max}^2$ . We should emphasize that the Online Dataset scales with the number of archetype components,  $M$ , and not the number of instantiated components in any (future) system,  $I$ , and with  $\mathcal{N}_{\max}^{\text{ports}}$ , and not  $\mathcal{N}_{\max}^{\text{com}}$ .

The Offline stage is expensive, and the Online Dataset extensive, for two reasons. First, we might have several or even many components in our library, and hence  $M$  may not be small. Second, we will *typically* have many port degrees of freedom:  $\mathcal{N}_{\max}^{\text{ports}}$  appears both in the formation/storage of the bubble affine decomposition, linearly, but also in the formation/storage of the Schur entry affine decomposition, *quadratically*. The first proliferation, in  $M$ , is shared by all RBE approaches; the second proliferation, in  $\mathcal{N}_{\max}^{\text{ports}}$ , is peculiar to the static condensation RBE approach – and a direct result of the “configuration agnostic” training of the library archetype components.

We close with a small technical remark. Our reduced basis error bounds require a coercivity lower bound, which, in the most general case, must be computed by the Successive Constraint Method (SCM) [18]. For some problems, in particular linear elasticity with high aspect ratio members, the Offline operation count can be considerable. However, in all cases, the contribution to both the Online Dataset memory and the Online operation count is negligible. (Indeed, only one Online SCM evaluation is required for each component in the Online stage). For this reason, and since the coercivity lower bound is entirely component local, we do not dwell further on this topic in the current paper.

### 6.3. Online stage

It shall be instructive to decompose the Online stage, and associated operation counts, into two parts. The first part entails (i) computation of all the reduced basis Schur complement entries (4.12), (4.13), and (ii) evaluation of all the reduced basis error bounds (5.10), (5.11). We shall denote the operation count associated with this part of the Offline stage by  $\tau_{\text{sc}}^{\text{RB}}$ . (Note in the next section we shall use this same  $\tau_{\text{sc}}^{\text{RB}}$  to denote computational timings associated with this part of the Online stage). The second part entails the solution of the reduced basis approximate Schur complement system of equations, (4.7), and evaluation of the minimum eigenvalue of the reduced basis approximate Schur complement,  $\tilde{\lambda}_{\min}$ , required in (5.19). We shall denote the operation count (and in Section 7, the computational timings) associated with this part of the Offline stage by  $\tau_S^{\text{RB}}$ . Note the total operation count/timing is simply the sum of  $\tau_{\text{sc}}^{\text{RB}}$ , the reduced basis contribution, and  $\tau_S^{\text{RB}}$ , the Schur complement contribution.

It is important to emphasize that both these operation counts/timings are defined as *marginal* operation counts/timings: the *additional* computational effort required to evaluate the reduced basis output and output error bound at the next step in a design sequence. Of course we include within this definition the important case in which we form and analyze for the first time – for a first parameter value – a new system constructed from our library. For our purposes below, we define  $I_{\text{eff}}$  to be the effective number of instantiated components in our computation, hence  $I_{\text{eff}} = \min(I'_{\text{cs}}, I'_{\text{var}})$ . Note that for a new system with no replicated components  $I_{\text{eff}} = I$ , whereas for either a new system with replicated components, or a parameter variation for an existing system, or a rearrangement of an existing system,  $I_{\text{eff}}$  “counts” only the number of instantiated components for which the component stiffness matrix must be (re)constructed. There are many important cases in which we can expect replicated components and perhaps even more cases – in particular within the interactive design or parameter estimation contexts – in which we would expect to vary only a few parameters in any given analysis step.

We now turn to  $\tau_{\text{sc}}^{\text{RB}}$  (interpreted here as an operation count, and in Section 7 as a timing):

$$\tau_{\text{sc}}^{\text{RB}} = I_{\text{eff}}(\mathcal{N}_{\max}^{\text{ports}}(Q_{\max} N_{\max}^2 + Q_{\max}^2 N_{\max}^2 + N_{\max}^3) + (\mathcal{N}_{\max}^{\text{ports}})^2 Q_{\max} N_{\max}^2). \quad (6.3)$$

Note the first term, which scales linearly with  $\mathcal{N}_{\max}^{\text{ports}}$ , reflects the computation of the reduced basis bubble coefficients, (4.2), and associated error bounds whereas the second term, which scales as  $(\mathcal{N}_{\max}^{\text{ports}})^2$ , reflects the evaluation of the reduced basis approximate Schur complement entries, (4.12). This strong dependence of  $\tau_{\text{sc}}^{\text{RB}}$  on the number of port degrees of freedom is a first and perhaps the most important motivation for a port reduction strategy [11]. We also note the beneficial effect of replication or incremental parameter variation through the prefactor  $I_{\text{eff}}$ .

We next turn to  $\tau_S^{\text{RB}}$  (interpreted here as an operation count, and in Section 7 as a timing). Here we do not provide an explicit operation count, but rather note that  $\tau_S^{\text{RB}}$  will of course depend at least linearly and in practice superlinearly with  $n_{\text{sc}}$ , the rank of the (reduced basis approximate) Schur complement. We recall that  $n_{\text{sc}}$  is the total number of degrees of freedom summed over all the global ports; the dependence of  $n_{\text{sc}}$  on  $\mathcal{N}_{\text{max}}^T$  is a second motivation for port reduction. We do note that the (reduced basis approximate) Schur complement has many nice features: the Schur complement will be sparse as dictated by the relatively few component neighbors with which any component is connected (through a shared global port); the Schur complement will be relatively well conditioned, with condition number  $O(1/h)$  [7]. We may thus consider solution (and eigensolution) by either sparse direct techniques or sparse preconditioned iterative techniques.

#### 6.4. Comparison framework

We shall compare our approach to two alternatives. Alternative I, characterized by operation count/timing  $\tau^{\text{I}}$ , is the static condensation truth Finite Element (FE) formulation described in Section 3. Alternative II, characterized by operation count/timing  $\tau^{\text{II}}$ , is a standard “global” truth finite formulation over  $X^h$ , (3.6). We make two remarks. First, we shall presume that we are in the real-time or many-query context such that we may plausibly consider in our comparison only the *Online* operation count, and Online Dataset requirements, of the static condensation RBE approach. (Of course, the Offline cost even in such situations can not be ludicrous, and in Section 7 we shall provide representative timings for the Offline stage as well). Second, we compare only operation counts/timing and not accuracy, as our rigorous error bounds in some sense ensure “equivalence” between the static condensation RBE and truth FE results.

We first consider Alternative I. We note that  $\tau^{\text{I}} = \tau_{\text{sc}}^{\text{FE}} + \tau_S^{\text{FE}}$ . The first term is given by

$$\tau_{\text{sc}}^{\text{FE}} = I_{\text{eff}}(\mathcal{N}_{\text{max}}^{\text{ports}} \mathcal{F}^{\text{FE}}(\mathcal{N}_{\text{max}}^{\text{com}}) + (\mathcal{N}_{\text{max}}^{\text{ports}})^2 C_{\text{sp}} \mathcal{N}_{\text{max}}^{\text{com}}), \quad (6.4)$$

where recall  $\mathcal{N}_{\text{max}}^{\text{com}}$  denotes the maximum number of truth FE degrees of freedom in a component over all components in a system, and  $\mathcal{F}^{\text{FE}}(\mathcal{N})$  denotes the operation count to solve a sparse finite element discrete system of size  $\mathcal{N}$  (note for our purposes here we may ignore the particular structure of the equations); also  $C_{\text{sp}}$  is a rough indication of the sparsity of the finite element discrete system in terms of the nonzero entries per row (for example, in three space dimensions we might expect  $C_{\text{sp}} \approx 20$  for a low-order finite element approximation). The second term,  $\tau_S^{\text{FE}}$ , is simpler:  $\tau_S^{\text{FE}} = \tau_S^{\text{RB}}$ .

We may thus conclude that if  $\tau_{\text{sc}}^{\text{RB}} \ll \tau_{\text{sc}}^{\text{FE}}$  then the static condensation RBE approach should be advantageous relative to the truth static condensation approach. (We implicitly assume here that  $\tau_{\text{sc}}^{\text{FE}}$  is at least of the same order as, and more likely much greater than,  $\tau_S^{\text{FE}}$ ; this “volume predominance” will typically be realized unless the components are mostly surfaces and hence ports). We directly observe from (6.3) and (6.4) that the operation counts for formation of the Schur complement for the reduced basis approximation and the truth finite element discretization include similar terms – a first term which scales as  $\mathcal{N}_{\text{max}}^{\text{ports}}$ , and a second term which scales as  $(\mathcal{N}_{\text{max}}^{\text{ports}})^2$ . Thus, the comparison  $\tau_{\text{sc}}^{\text{RB}}$  versus  $\tau_{\text{sc}}^{\text{FE}}$  reduces to the standard “reduced basis calculus”: if  $N_{\text{max}} \ll \mathcal{N}_{\text{max}}^{\text{com}}$  we anticipate that  $\tau_{\text{sc}}^{\text{RB}} \ll \tau_{\text{sc}}^{\text{FE}}$ . In fact, we expect the static condensation formulation to further tip the balance in favor of reduced basis treatment: our port functions are designed to decay rapidly into the interior of the component and should thus arguably depend relatively weakly on the parameters; the latter, in turn, suggests relatively small  $N_{\text{max}}$ . In Section 7 we will provide numerical evidence which supports this claim (at least for our particular examples).

We next consider Alternative II. It is in general difficult to make a direct comparison between the static condensation RBE approach and a standard global finite element discretization. First, from a theoretical perspective, the comparison can be very problem dependent (as regards degrees of freedom, sparsity, and condition number) and also “solver-dependent”; second, from an empirical perspective, the comparison may be very cumbersome – by construction, the static condensation reduced basis element approach avoids global quantities and instead considers solely  $I$ -tuples. For these two reasons, both in this section and Section 7, we consider a simple sufficient condition, rather than a more complicated necessary condition, under which the static condensation RBE approach will be much more efficient than a standard global finite element approach.

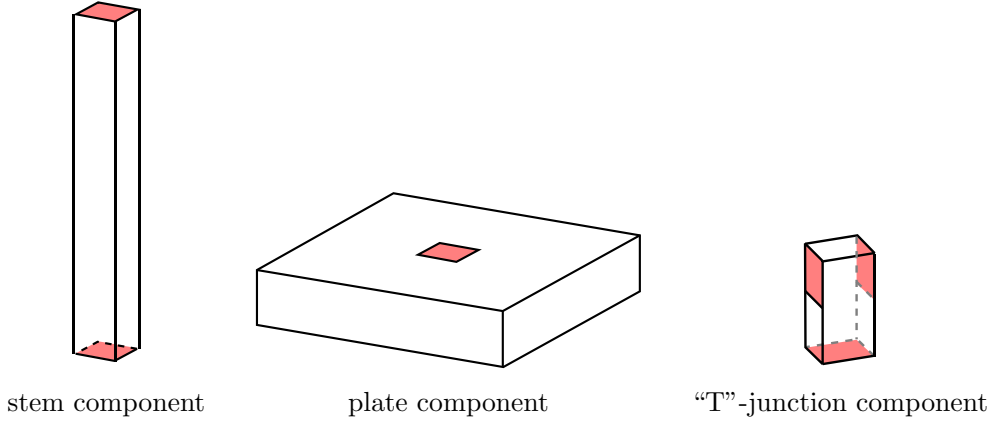


FIGURE 4. Three archetype components for the thermal fin library: a stem, a plate, and a “T”-junction. Ports are shaded in red.

In particular, we claim that if  $\tau_{\text{sc}}^{\text{RB}}$  is of the same order of magnitude as (or at least not much larger than)  $\tau_{\text{S}}^{\text{RB}}$ , then – again presuming “volume predominance” – the static condensation RBE approach will be considerably faster than a standard global truth finite element formulation. The argument:  $\tau_{\text{sc}}^{\text{RB}} + \tau_{\text{S}}^{\text{RB}} \approx \tau_{\text{S}}^{\text{RB}} = \tau_{\text{S}}^{\text{FE}}$  will be much smaller than  $\tau^{\text{II}} = \mathcal{F}^{\text{FE}}(\mathcal{N}^{\text{tot}})$  given that  $n_{\text{sc}}$  will be much smaller than  $\mathcal{N}^{\text{tot}} \equiv \dim(X^h)$ . Inspection of the  $\tau_{\text{sc}}^{\text{RB}}$  of (6.3) suggests that in cases in which  $I_{\text{eff}}$  is small compared to  $I$ , and hence in which  $I_{\text{eff}} \mathcal{N}_{\text{max}}^{\text{ports}}$  is small compared to  $n_{\text{sc}}$ ,  $\tau_{\text{sc}}^{\text{RB}}$  should indeed be small compared  $\tau_{\text{S}}^{\text{RB}}$ . In Section 7 we shall provide numerical evidence which supports this claim (at least for our particular examples).

## 7. NUMERICAL RESULTS

In this section we present numerical results to demonstrate the capabilities of the static condensation RBE method. We present results for model problems from heat transfer and solid mechanics. The results presented here are obtained with `rb00mit` [23], `libMesh` [22], and Matlab.

### 7.1. Heat transfer: thermal fin library

We consider here a library with which we can subsequently build a variety of “thermal fin” systems. Note the ultimate application, here thermal fins, dictates both the underlying physics and hence bilinear/linear form, but also typically the kinds of geometries, geometric variations, and port connectivities which must be anticipated. These components are shown schematically in Figure 4. We shall discuss the stem archetype in detail, and then we consider the plate and “T”-junction more briefly.

The dimensional physical domain for the stem archetype component,  $m = 1$ , is of width  $0.4W$  and height  $3\tilde{H}W$ , where  $W$  is a dimensional length scale. We then non-dimensionalize to obtain the physical domain  $\hat{\Omega}_1^o(\hat{\mu}_1^{\text{geo}}) = (0, 0.4) \times (0, 0.4) \times (0, 3\tilde{H}) \subset \mathbb{R}^3$ . We then set  $\hat{\mu}_1^{\text{geo}} = \tilde{H}$  with  $\hat{\mathcal{D}}_1^{\text{geo}} = [2/3, 4/3]$ . As shown in Figure 4, this component has two ports,  $\hat{\gamma}_{1,1}^o(\hat{\mu}_1^{\text{geo}}) \equiv (0, 0.4) \times (0, 0.4) \times \{0\}$  and  $\hat{\gamma}_{1,1}^o(\hat{\mu}_1^{\text{geo}}) \equiv (0, 0.4) \times (0, 0.4) \times \{3\tilde{H}\}$ . Note that there are also docking parameters (translation, rotation) that are implicitly associated with the stem component but which we do not explicitly list. We also introduce the associated reference domain  $\Omega_{m=1} \equiv \hat{\Omega}_1^o(\hat{\mu}_1^{\text{geo,ref}} = 1) = (0, 0.4) \times (0, 0.4) \times (0, 3)$ ; this domain is meshed with  $4 \times 4 \times 30$   $Q_1$  ( $d = 3$ ) elements.

We consider equilibrium heat conduction for this archetype component with heat transfer from the component surface to the ambient and subject to uniform volumetric heat generation  $\dot{q}$ . Hence we introduce the thermal conductivity  $k_{\text{th}}$ , nondimensional conductivity ratio  $\kappa = k_{\text{th}}/k_{\text{th}}^0$  (where  $k_{\text{th}}^0$  denotes a nominal conductivity),

heat transfer coefficient  $h_{\text{th}}$ , and Biot number  $\text{Bi} = h_{\text{th}}W/k_{\text{th}}$ . The coefficient parameters are then given by  $\hat{\mu}_1^{\text{coeff}} = (\text{Bi}, \kappa)$ , and we set  $\hat{\mathcal{D}}_1^{\text{coeff}} = [0.001, 0.01] \times [0.5, 2]$ .

We define nondimensional  $x$  as  $x/W$ , and we introduce the nondimensional temperature  $u \equiv k_{\text{th}}^0(T - T_{\text{ambient}})/(\hat{q}W^2)$ . Then on the physical domain we have the nondimensionalized PDE

$$-\kappa \Delta u = 1 \quad \text{over} \quad \hat{\Omega}_1^o(\hat{\mu}_1^{\text{geo}}), \quad (7.1)$$

$$\kappa \frac{\partial u}{\partial n} = -\kappa \text{Bi} u \quad \text{on} \quad \partial \hat{\Omega}_1^o(\hat{\mu}_1^{\text{geo}}), \quad (7.2)$$

where  $\partial \hat{\Omega}_1^o(\hat{\mu}_1^{\text{geo}})$  denotes the boundary of  $\hat{\Omega}_1^o(\hat{\mu}_1^{\text{geo}})$ . We now consider the corresponding forms reformulated for the archetype reference domain.

We have

$$a_1(v, w; \hat{\mu}_1) \equiv \sum_{q=1}^5 \Theta_{a_1}^q(\hat{\mu}_1) a_1^q(v, w), \quad (7.3)$$

where (note that we avoid  $\hat{\mu}_1^{\text{geo}}$  and  $\hat{\mu}_1^{\text{coeff}}$  in favor of  $\tilde{H}$ ,  $\text{Bi}$  and  $\kappa$  for the sake of clarity in the functions presented below)

$$\Theta_{a_1}^1(\hat{\mu}_1) \equiv \kappa \tilde{H}, \quad \Theta_{a_1}^2(\hat{\mu}_1) \equiv \kappa / \tilde{H}, \quad \Theta_{a_1}^3(\hat{\mu}_1) \equiv \text{Bi} \kappa \tilde{H}, \quad \Theta_{a_1}^4(\hat{\mu}_1) \equiv P_1 \text{Bi} \kappa, \quad \Theta_{a_1}^5(\hat{\mu}_1) \equiv P_2 \text{Bi} \kappa, \quad (7.4)$$

and

$$a_1^1(v, w) \equiv \int_{\Omega_1} (v_x w_x + v_y w_y), \quad (7.5)$$

$$a_1^2(v, w) \equiv \int_{\Omega_1} v_z w_z, \quad (7.6)$$

$$a_1^3(v, w) \equiv \int_{\partial \Omega_1 \setminus (\gamma_{1,1} \cup \gamma_{1,2})} vw, \quad (7.7)$$

$$a_1^4(v, w) \equiv \int_{\gamma_{1,1}} vw, \quad (7.8)$$

$$a_1^5(v, w) \equiv \int_{\gamma_{1,2}} vw; \quad (7.9)$$

also, we define a volumetric source term on  $\Omega_1$ ,

$$f_1(v; \mu) \equiv \tilde{H} \int_{\Omega_1} v. \quad (7.10)$$

Recall that all these forms are defined over the archetype reference domain, and hence the appearance of the geometric parameter  $\tilde{H}$ .

We employ for the  $\Omega_1$  inner product

$$(v, w)_{X_1} \equiv \int_{\Omega_1} (v_x w_x + v_y w_y) \kappa_{\min} \tilde{H}_{\min} + (v_z w_z) \kappa_{\min} / \tilde{H}_{\max}, \quad (7.11)$$

where  $\tilde{H}_{\min} = 2/3$ ,  $\tilde{H}_{\max} = 4/3$ , and  $\kappa_{\min} = 0.5$ . With this choice we may set  $\alpha_{1;0}^{h,\text{LB}} \equiv 1$  for the coercivity constant lower bound; note the coercivity constant is defined with respect to the *bubble space*  $B_{1;0}^h$  and hence the semi-norm in (7.11) suffices.

We observe that the operators  $a_1^4$  and  $a_1^5$  vanish for all  $v, w \in B_{1,0}^h$ ; these terms are included in the formulation to permit us to impose general natural boundary conditions on the ports *via* the interface functions. To wit, we include the scalars  $P_1, P_2 \in \{0, 1\}$  in order to turn the port Biot terms “on” or “off” as desired. For example, we would set  $P_1 = 0$  if a stem component has a connection on port  $\gamma_{1,1}$ ; similarly, we would set  $P_1 = 0$  if there is no connection on  $\gamma_{1,1}$  and we wish to impose a homogeneous Neumann condition on  $\gamma_{1,1}$ . On the other hand, we would set  $P_1 = 1$  if we wish to impose a Robin condition on  $\gamma_{1,1}$ . In essence, we take advantage of the general port treatment to impose general boundary conditions. We note that  $P_1$  and  $P_2$  are similar to docking parameters in the sense that they do not affect the component-level RB approximations.

The other two components of the heat transfer Library represent similar physics but in different geometries; we shall define the geometric domains and parameters for these components, but omit the component operator equations for the sake of brevity. Let  $m = 2$  denote the plate archetype component, with the non-dimensional physical domain  $\hat{\Omega}_{m=2}^o(\hat{\mu}_{m=2}^{\text{geo}}) \equiv (0, 2\tilde{W} + 0.4) \times (0, 2\tilde{W} + 0.4) \times (0, \tilde{H}/2)$ . The plate has two ports at  $\hat{\gamma}_{2,1}^o(\hat{\mu}_2^{\text{geo}}) \equiv (\tilde{W}, \tilde{W} + 0.4) \times (\tilde{W}, \tilde{W} + 0.4) \times \{0\}$  and  $\hat{\gamma}_{2,2}^o(\hat{\mu}_2^{\text{geo}}) \equiv (\tilde{W}, \tilde{W} + 0.4) \times (\tilde{W}, \tilde{W} + 0.4) \times \{\tilde{H}/2\}$ . In this case we define  $\hat{\mu}_2^{\text{geo}} = (\tilde{H}, \tilde{W})$  and  $\hat{\mathcal{D}}_2^{\text{geo}} \equiv [2/3, 4/3] \times [0.5, 2]$ . The plate reference geometry is given by  $\Omega_{m=2} = \hat{\Omega}_2^o(\hat{\mu}_2^{\text{geo}} = (1, 1)) = (0, 2.4) \times (0, 2.4) \times (0, 0.5)$ , and this domain is meshed with  $24 \times 24 \times 5$   $Q_1$  ( $d = 3$ ) elements. The coefficient parameters for the plate are  $\hat{\mu}_2^{\text{coeff}} = (\text{Bi}, \kappa)$ , with domain  $\hat{\mathcal{D}}_2^{\text{coeff}} \equiv [0.001, 0.01] \times [0.5, 2]$ . Also, we set  $f_2 \equiv 0$ . Similarly, let  $m = 3$  denote the “T”-junction archetype component. In this case there is no geometric variation so that  $\Omega_{m=3} = \hat{\Omega}_3^o \equiv (0, 0.4) \times (0, 0.4) \times (0, 0.8)$ . The geometry is meshed with  $4 \times 4 \times 8$   $Q_1$  ( $d = 3$ ) elements. The “T” component has three ports:  $\gamma_{3,1} \equiv (0, 0.4) \times (0, 0.4) \times \{0\}$ ,  $\gamma_{3,2} \equiv (0, 0.4) \times \{0\} \times (0.4, 0.8)$ , and  $\gamma_{3,3} \equiv (0, 0.4) \times \{0.4\} \times (0.4, 0.8)$ . This component has coefficient parameters  $\hat{\mu}_3^{\text{coeff}} = (\text{Bi}, \kappa)$  with associated parameter domain  $\hat{\mathcal{D}}_3^{\text{coeff}} \equiv [0.001, 0.01] \times [0.5, 2]$ . We set  $f_3$  to be a uniform volumetric source term analogous to  $f_1$ .

We note that for  $m = 1, 2, 3$ , the thermal conductivity parameter scales out of (4.2). This can be seen (in the  $m = 1$  case) from the presence of the  $\kappa$  factor in each  $\Theta_{a_1}^q$  in (7.4): thus  $a_1$  scales linearly with  $\kappa$ , and hence from (4.2) the bubble is independent of  $\kappa$ . (Note to achieve this independence we scale the Biot number by the  $k_{\text{th}}$  rather than  $k_{\text{th}}^0$  to get a  $\kappa$  factor on both sides of (7.2)). Therefore, the thermal conductivity is a “free” parameter with regards to the reduced basis approximation for the bubble functions of (4.2). In fact, it is not only free as regards the cost of the RB approximation, but also free in the sense that  $\mu_3$  can take on any positive value quite independent of the definition of  $\hat{\mathcal{D}}_1$ . Note that the docking parameters and additionally  $P_1, P_2$  are also “free” – in the sense that these free parameters are handled by the Schur complement rather than the RB approximation.

We now perform the Offline stage for this library of three thermal fin components. We have 25 nodes on each port, hence  $\mathcal{N}_1^{\text{ports}} = \mathcal{N}_2^{\text{ports}} = 50$ , and  $\mathcal{N}_3^{\text{ports}} = 75$ . For each component, we set the (absolute) tolerance for termination of the Greedy algorithm to  $10^{-5}$ , and we also set the limit for the dimension of each RB space to  $N_{\text{lim}} = 15$ . We present in Figure 5 a plot of  $\dim(\tilde{B}_{1,1,k;0})$  for  $1 \leq k \leq 25$ . We do observe that in general the dimensions of the RB spaces are relatively low and furthermore that the dimensions of the RB spaces appear to slightly decrease with  $k$  – as suggested by the decay of the  $\psi_{i,j,k} + \tilde{b}_{i,j,k}(\mu_i)$  into component interiors. Note that the  $m = 2$  component has one more parameter and more complicated geometric variations; as a result, in this case all RB spaces saturate at the  $N_{\text{lim}} = 15$  limit. Also, we note the total offline times for each component: 157 s for  $m = 1$ ; 5750 s for  $m = 2$ ; 6 s for  $m = 3$ .

We now consider the Online stage. In all cases we use the maximum RB space dimension (*i.e.*, at most  $N_{\text{lim}} = 15$ ). To demonstrate the flexibility of the static condensation RBE method we shall assemble and solve several different systems from the three reference components introduced above. We first consider System<sub>1</sub> which has 6 stem components and 5 plates –  $I = 11$  with six instantiations of archetype component 1 and five instantiations of archetype component 2. We “stack” the components vertically in the order (starting at the base) stem<sub>1</sub> → plate<sub>1</sub> → stem<sub>2</sub> → plate<sub>2</sub> → ... → stem<sub>6</sub>, where  $\mathcal{M}(1) = \dots = \mathcal{M}(6) = 1$ ,  $\mathcal{M}(7) = \dots = \mathcal{M}(11) = 2$ . We also introduce two system outputs:  $s_1(\mu)$  is the average temperature over the base port of stem<sub>1</sub>, and  $s_2(\mu)$

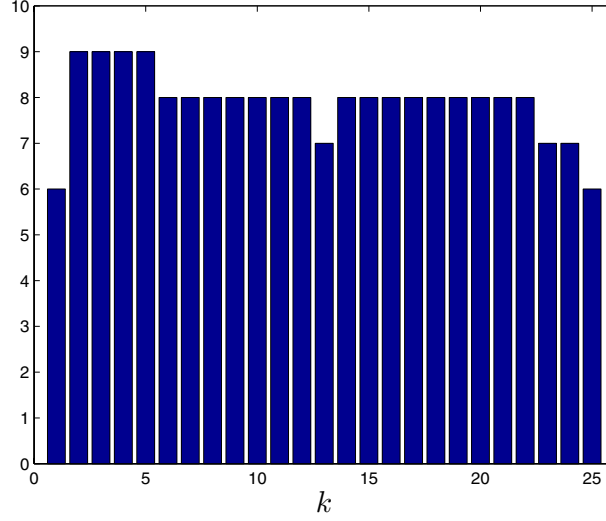


FIGURE 5. The dimension of the RB bubble spaces on port  $\gamma_{1,1}$ :  $\dim(\tilde{B}_{1,1,k;0})$ , for  $1 \leq k \leq 25$ .

is the average temperature on the top port of stem<sub>3</sub>. System<sub>1</sub> has 38 parameters in total, and there are no geometric constraints so  $\mathcal{D}^{\text{geo}}$  is simply the tensor product of the  $\hat{\mathcal{D}}_{\mathcal{M}(i)}^{\text{geo}}$ .

For our first analysis, the stem parameters are

$$\begin{aligned} \mu_{\text{stem}_1} = \mu_1 &= (0.67; 0.01, 1.2), & \mu_{\text{stem}_2} = \mu_2 &= (1; 0.0075, 1), & \mu_{\text{stem}_3} = \mu_3 &= (1.33; 0.002, 0.5), \\ \mu_{\text{stem}_4} = \mu_4 &= (1.33; 0.002, 0.5), & \mu_{\text{stem}_5} = \mu_5 &= (1; 0.0075, 1), & \mu_{\text{stem}_6} = \mu_6 &= (0.67; 0.01, 1.2); \end{aligned} \quad (7.12)$$

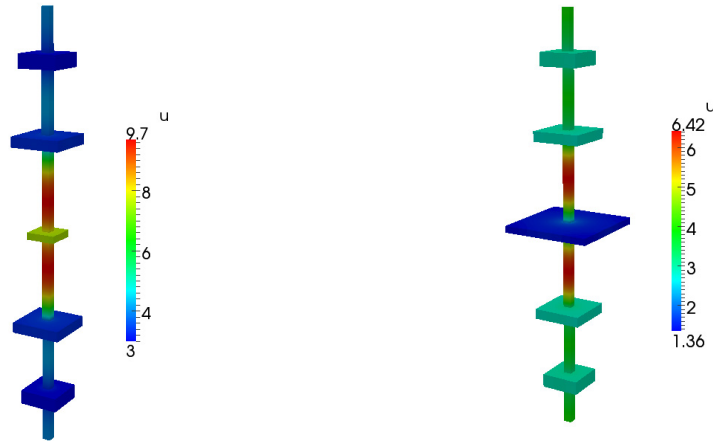
and the plate parameters are

$$\begin{aligned} \mu_{\text{plate}_1} = \mu_7 &= (1.33, 0.75; 0.01, 1), & \mu_{\text{plate}_2} = \mu_8 &= (1, 1; 0.01, 1), & \mu_{\text{plate}_3} = \mu_9 &= (0.67, 0.5; 0.005, 1), \\ \mu_{\text{plate}_4} = \mu_{10} &= (1, 1; 0.01, 1), & \mu_{\text{plate}_5} = \mu_{11} &= (1.33, 0.75; 0.01, 1). \end{aligned} \quad (7.13)$$

We set  $P_1 = 1$  and  $P_2 = 1$  in order to impose a heat transfer (Robin) boundary condition on the bottom port of stem<sub>1</sub> and the top port of stem<sub>6</sub>.

The system temperature profile is shown in Figure 6A; the associated RB system outputs are  $\tilde{s}_1(\mu) = 4.10$ ,  $\tilde{s}_2(\mu) = 7.85$ . We obtain the field output bound  $\Delta^{\text{U}}(\mu) = 0.14$ , and the system output error bound  $\Delta^s(\mu) = 0.34$  for both  $\tilde{s}_1(\mu)$  and  $\tilde{s}_2(\mu)$ . The true field error is  $\|\mathbb{U}(\mu) - \tilde{\mathbb{U}}(\mu)\|_2 = 4.06 \times 10^{-5}$ . The effectivity of the error bound  $\Delta^{\text{U}}(\mu) / \|\mathbb{U}(\mu) - \tilde{\mathbb{U}}(\mu)\|_2 = 3.40 \times 10^3$  is quite poor; however, when we employ the sharper error bound  $\Delta_*^{\text{U}}(\mu)$  we obtain an effectivity  $\Delta_*^{\text{U}}(\mu) / \|\mathbb{U}(\mu) - \tilde{\mathbb{U}}(\mu)\|_2 = 1.37 \times 10^2$ , which is certainly improved and commensurate with standard RB error bound effectivities reported in the literature. We anticipate that the effectivity will increase as the size of the system,  $n_{\text{sc}}$ , increases – which in turn could necessitate compensating increases in the dimension of the RB spaces. However, the improved bound should mitigate the effect by exploiting the decay of the port degree of freedom coefficients.

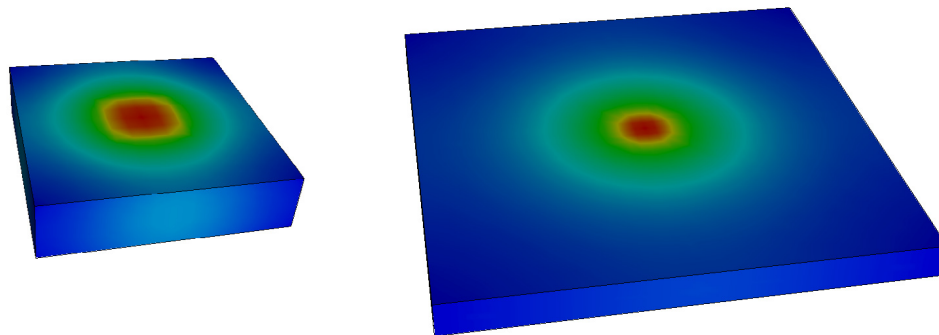
The Online computation time in this case is 0.72 s, with  $\tau_{\text{sc}}^{\text{RB}} = 0.67$  and  $\tau_{\text{S}}^{\text{RB}} = 0.05$ . The truth static condensation approach (Alternative I) requires  $\tau_{\text{sc}}^{\text{FE}} = 191$  s in this case, and hence the RB approach yields a speedup factor of roughly 265. Also, since  $\tau_{\text{S}}^{\text{RB}}$  is only a factor of roughly 13 smaller than  $\tau_{\text{sc}}^{\text{RB}}$ , we plausibly satisfy our sufficient condition from Section 6 for the static condensation RBE approach to be much more efficient than a standard global finite element approach (Alternative II). Indeed, the static condensation system is of dimension  $n_{\text{sc}} = 300$  – compared to  $\dim(X^h) = 38\,900$ ; we enjoy here the benefits of the “quasi-one-dimensional” limit with relatively few port degrees of freedom compared to interior degrees of freedom.



(A) Solution  $\tilde{u}^o(\mu)$  over  $\Omega^o(\mu^{\text{geo}})$  for parameters defined in (117), (118); minimum is 3.0 (blue), maximum is 9.7 (red).

(B) Solution  $\tilde{u}^o(\mu)$  over  $\Omega^o(\mu^{\text{geo}})$  for the parameters defined in (117), (118), except that  $\tilde{W} = 2$  (rather than 0.5) for plate 3; minimum is 1.36 (blue), maximum is 6.42 (red).

FIGURE 6. Temperature profiles for our system with 6 stems and 5 plates for two different values of the parameters.



(A) Detail of plate<sub>3</sub> from Figure 6A; minimum is 7.52 (blue), maximum is 7.90 (red).

(B) Detail of plate<sub>3</sub> from Figure 6B; minimum is 1.36 (blue), maximum is 2.20 (red).

FIGURE 7. Temperature profiles for our system with 6 stems and 5 plates: detail for the middle plate.

We next demonstrate a “parameter sweep”: we predict the field and outputs of our system as we vary the “horizontal scaling” parameter  $\tilde{W}$  for plate<sub>3</sub> from 0.5 to 2; we hold all other parameters fixed per (7.12), (7.13), and hence now  $I_{\text{eff}} = 1$ . Figure 6A presents the temperature field for  $\tilde{W} = 0.5$ , while Figure 6B presents the temperature profile for  $\tilde{W} = 2$ ; Figures 7A and 7B provide a “zoomed-in view” of plate<sub>3</sub> extracted from Figures 6A and 6B, respectively. We note that the change in  $\tilde{W}$  results in a significant change in the overall temperature as well as the temperature distribution. We show in Figure 8 the system output  $\tilde{s}_2(\mu)$  and associated



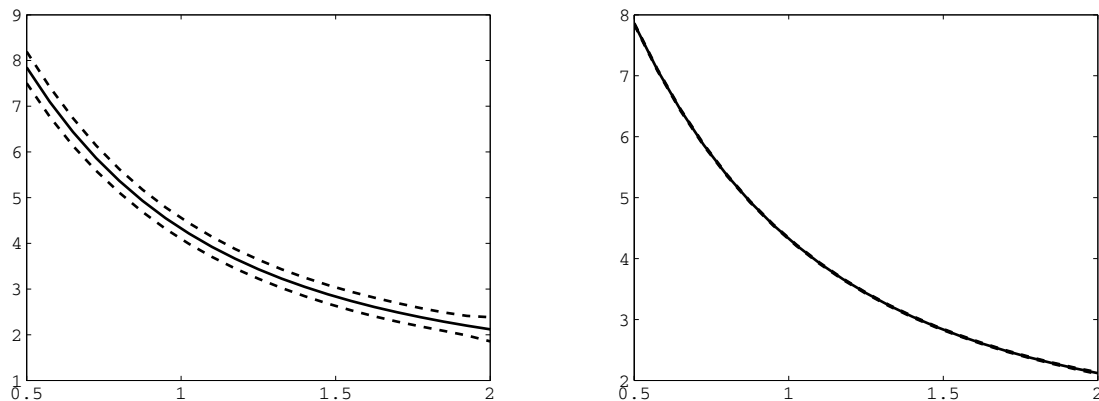


FIGURE 8. Plot of  $\tilde{s}_2(\mu)$  (solid line) and error bounds (dashed lines) at 21 evenly spaced parameters for the plate<sub>3</sub> horizontal scaling parameter  $\tilde{W}$  in the range  $[0.5, 2]$  – all other parameters are as defined in (7.12), (7.13). The output error bounds in the left and right plots are based on  $\Delta^s(\mu)$  and  $\Delta_*^s(\mu)$ , respectively.

output error bounds at 21 parameters in the range  $[0.5, 2]$ ; the error bounds confirm good accuracy in each case. In this case we have  $\tau_{sc}^{RB} = 0.10$  s, which is now only twice  $\tau_S^{RB}$ , and hence the static condensation RBE is clearly advantageous with respect to both a truth static condensation approach (Alternative I) and a global finite element approach (Alternative II).

We now consider a new system, System<sub>2</sub>, which has many repeated components. We instantiate 15 stems and 14 plates and stack them in the same way (stem  $\rightarrow$  plate  $\rightarrow$  stem) as in System<sub>1</sub>. In this case we set zero Neumann boundary conditions on the bottom and top ports of stem<sub>1</sub> and stem<sub>15</sub>, respectively. This system accommodates up to 101 independent parameters, however for our homogeneous system we set each stem parameter to  $\mu_{stem} \equiv (1; 0.01, 1)$ , and each plate parameter to  $\mu_{plate} \equiv (1, 1; 0.008, 1)$ . The solution field is shown in Figure 9A; we obtain a relative error bound of  $\Delta^U(\mu)/\|\tilde{U}(\mu)\|_2 = 0.010$ . In this case we have  $I_{eff} = 2$ , and  $\tau_{sc}^{RB} = 0.12$  s compared to  $\tau_S^{RB} = 0.14$  s. The dimension of the static condensation system is  $n_{sc} = 750$  – compared to  $\dim(X^h) = 107\,500$ . This case with many repeated components unequivocally satisfies our sufficient condition for the static condensation RBE approach to be much more efficient than a standard global finite element approach.

As our next example we consider a system System<sub>3</sub> which is a rearrangement of System<sub>2</sub> (recall our definition of a rearrangement from Sect. 6). We now disconnect stem<sub>4</sub> from plate<sub>4</sub> to introduce a “crack,” and we set  $P_2 = 0$  to impose a zero Neumann condition on the crack. This yields a slightly larger static condensation system,  $n_{sc} = 775$ . The temperature field in this case is shown in Figure 9B: the crack leads to a significantly higher temperature in stem<sub>4</sub>, as expected; the accuracy of the prediction is confirmed by the relative error bound  $\Delta^U(\mu)/\|\tilde{U}(\mu)\|_2 = 0.0102$ . Since System<sub>3</sub> is a rearrangement of System<sub>2</sub> (the immediately preceding simulation), we obtain  $I_{eff} = 0$ , and  $\tau_{sc}^{RB} = 0$  s,  $\tau_S^{RB} = 0.14$  s. This example illustrates the ease with which we may consider topology variations.

Finally, as our last thermal case we construct the system shown in Figure 10 which contains all three types of reference components: the system contains 7 stems, 3 plates, and 3 “T”-junction components, with parameters set as follows

$$\begin{aligned} \mu_{stem_1} &\equiv (1; 0.01, 1), & \mu_{stem_2} &\equiv (1; 0.01, 1.25), & \mu_{stem_3} &\equiv (1; 0.01, 1), & \mu_{stem_4} &\equiv (1; 0.01, 1.2), \\ \mu_{stem_5} &\equiv (1; 0.005, 1), & \mu_{stem_6} &\equiv (0.7; 0.01, 1), & \mu_{stem_7} &\equiv (0.7; 0.01, 1), \\ \mu_{plate_1} &\equiv (1, 1; 0.01, 1), & \mu_{plate_2} &\equiv (1, 0.8; 0.008, 1.2), & \mu_{plate_3} &\equiv (1, 1; 0.01, 1), \\ \mu_{T-junction_1} &\equiv (0.01, 1), & \mu_{T-junction_2} &\equiv (0.001, 1), & \mu_{T-junction_3} &\equiv (0.005, 1). \end{aligned}$$

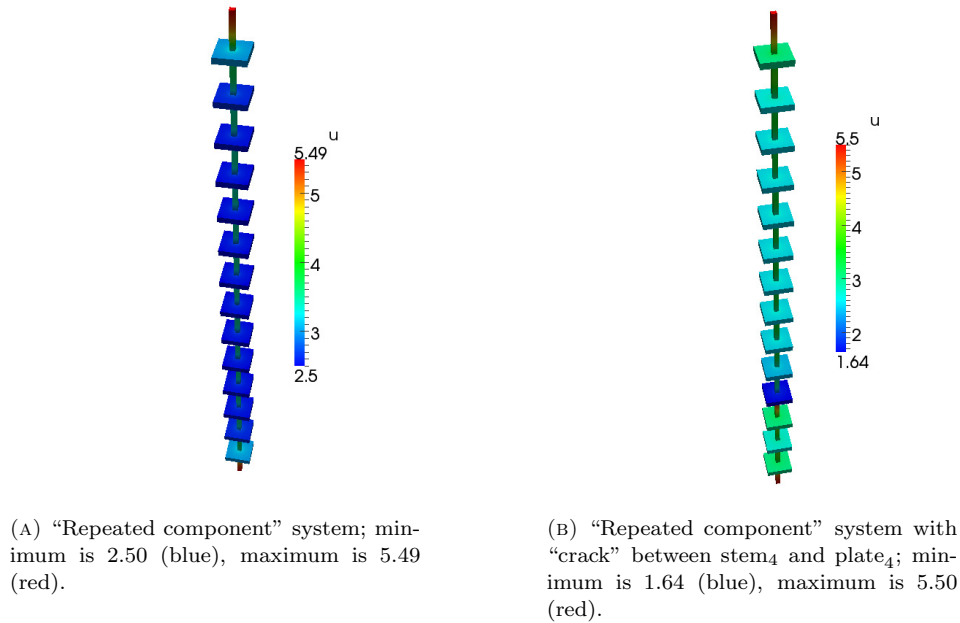


FIGURE 9. Temperature fields for two system configurations with 15 identical stems and 14 identical plates.

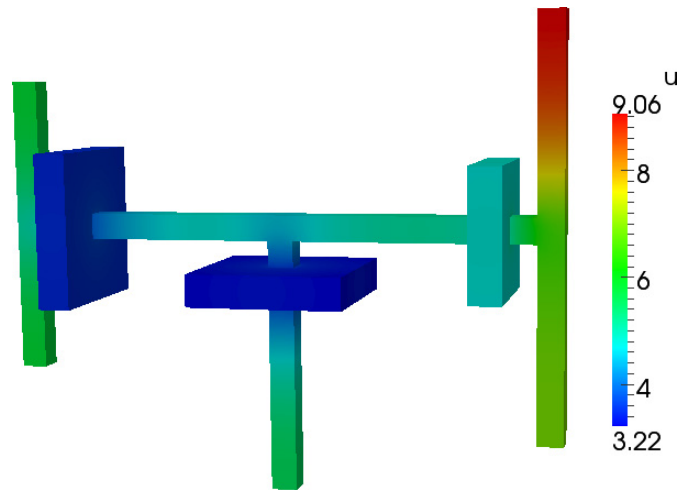


FIGURE 10. Temperature field for a system which contains all three types of thermal components; minimum is 3.22 (blue), maximum is 9.06 (red).

The temperature field is shown in Figure 10, and we obtain the relative error bound  $\Delta^U(\mu)/\|\tilde{U}(\mu)\|_2 = 0.014$ . Here the total Online computation time is 0.56 s, with  $\tau_{sc}^{RB} = 0.47$  s and  $\tau_S^{RB} = 0.09$  s;  $n_{sc} = 425$  compared to  $\dim(X^h) = 26,425$ . This example illustrates the good side of the curse of dimensionality: we obtain combinatorial flexibility in system design but cost increases only algebraically.

Note that in the thermal fin examples above we employ the heat transfer coefficient as a simple (but typically quite effective) engineering approximation for the much more difficult coupled conduction/fluid flow problem in

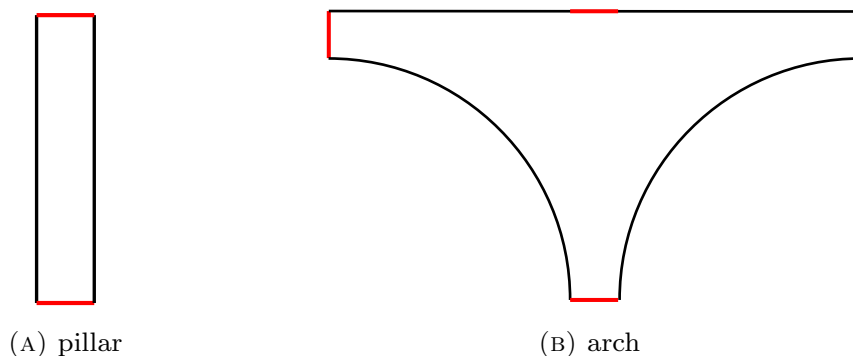


FIGURE 11. The two components of the historic structure library: the first archetype component is a pillar, the second archetype component is an arch. Ports are shaded in red.

the fin and the surrounding air. The latter is not amenable to our techniques due a fundamental, and perhaps the main, limitation of our approach: linearity as required by the static condensation procedure.

## 7.2. Linear elasticity: historic structure library

We now move to the solid mechanics example. In this case, the solution is a vector field of displacements. The port mode and interface function constructions directly apply to this case, except that we now solve vector problems in (3.8) and (3.11), (3.12), (3.13). In this case, well-posedness of the Schur complement system relies on Korn’s inequality, and we do not analyze this issue here – though we do note that our *a posteriori* error bound results in Propositions 5.3 and 5.6 still apply.

We consider the two archetype components shown in Figure 11: (i) a “pillar” component, and (ii) an “arch” component. The dimensional physical domain of the pillar archetype component,  $m = 1$ , is  $(0, W) \times (0, 5\tilde{H}W)$ , where  $W$  is a dimensional length scale. We then non-dimensionalize to obtain the physical domain  $\hat{\Omega}_{m=1}^o(\hat{\mu}_{m=1}^{\text{geo}}) = (0, 1) \times (0, 5\tilde{H})$  as shown in Figure 11A. The pillar has two ports corresponding to the bottom and top boundaries of the domain, respectively. We consider  $\hat{\mu}_1^{\text{geo}} = \tilde{H}$  and the domain  $\hat{\mathcal{D}}_1^{\text{geo}} \equiv [0.02, 2.0]$ . We set  $\Omega_{m=1} = \hat{\Omega}_1^o(\hat{\mu}_1^{\text{geo}} = 1)$ . We consider equilibrium elasticity on the archetype component (we also permit translations but not rotations) for a linear isotropic medium with Young’s modulus  $\tilde{E}E^0$  (nominal Young’s modulus  $E^0$ ) subject to a uniform body force  $\tilde{\rho}\rho^0g$  (nominal density  $\rho^0$ , acceleration of gravity  $g$ ) in the (negative) vertical direction. We introduce the coefficient parameters  $\hat{\mu}_1^{\text{coeff}} = (\tilde{E}, \tilde{\rho})$  and the corresponding coefficient parameter domain is  $\hat{\mathcal{D}}_1^{\text{coeff}} \equiv [1, 10] \times [10^{-7}, 10^{-6}]$ . (The small magnitude of  $\tilde{\rho}$  is due to the ratio of gravitational and elastic stress effects for realistic values of the Young’s modulus). We refer to [28] for the construction of the operators; the affine forms are recovered with  $Q_{a_1} = 3$  and  $Q_{f_1} = 1$ . The nondimensional displacement is scaled by  $\rho^0gW^2/E^0$ .

Let  $m = 2$  denote the arch archetype component with domain  $\Omega_{m=2} = \hat{\Omega}_2^o$  as shown in Figure 11B; this component has no geometric parameters. The arch has four ports corresponding to the four boundaries shown in Figure 11B. We consider two (non-dimensional) coefficient parameters:  $\mu_2^{\text{coeff}} = (\tilde{E}, \tilde{\rho})$  with domain  $\hat{\mathcal{D}}_2^{\text{coeff}} \equiv [1, 10] \times [10^{-7}, 10^{-6}]$ . The physical model is again a linear isotropic medium subject to a uniform body force. Given the absence of geometric variations,  $Q_{a_2} = Q_{f_2} = 1$ .

For both  $m = 1$  and  $m = 2$  the parameters corresponding to the Young’s modulus and the material density are both free. The  $m = 2$  component is particularly simple: the Young’s modulus  $\tilde{E}$  scales  $a$  in both (4.1) and (4.2); the material density  $\tilde{\rho}$  scales (only) the right-hand side of (4.1). It follows that for  $m = 2$  there are in fact no “real” parameters: in (4.1), the bubble functions scale as  $1/\tilde{\rho}$ ; in (4.2) the bubble function scales as  $\tilde{\rho}/\tilde{E}$ .

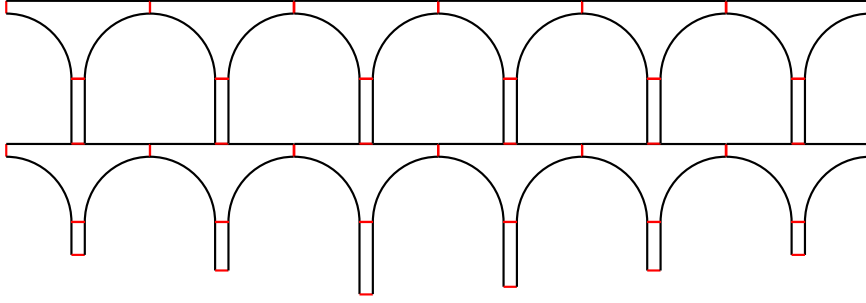


FIGURE 12. The “pont du Gard” bridge structure.

We now perform the Offline stage for the two components in our library. We have 5 nodes on each port, and since the problem is defined for a vector (displacement field), we obtain  $\mathcal{N}_1^{\text{ports}} = 20$  and  $\mathcal{N}_2^{\text{ports}} = 40$ . We set the (relative) tolerance for termination of the Greedy algorithm for each component to  $10^{-5}$  or  $N_{\text{lim}} = 15$ . For the pillar component we obtain  $\dim(\tilde{B}_{1,j,k;0}) = 15$  for each  $j \in \{1, 2\}$ ,  $1 \leq k \leq 10$ . For the arch component we obtain only one basis function in each RB bubble space: the RB Greedy algorithm detects the free parameters automatically.

We then consider the Online stage. In all cases we use the full RB dimension available. We first consider a “pont du Gard” system,  $\text{System}_1$ , consisting of four layers of components stacked as shown in Figure 12. The first and the third layers have 6 pillar components each; and the second and fourth layers have 6 arch components each. The ordering of the first and second layers are  $\text{pillar}_1 \rightarrow \text{pillar}_2 \rightarrow \dots \rightarrow \text{pillar}_6$ , and  $\text{arch}_1 \rightarrow \text{arch}_2 \rightarrow \dots \rightarrow \text{arch}_6$ , respectively, from the left to the right; similarly, the ordering for the third and fourth layers are  $\text{pillar}_7 \rightarrow \dots \rightarrow \text{pillar}_{12}$  and  $\text{arch}_7 \rightarrow \dots \rightarrow \text{arch}_{12}$ . We also introduce our system output:  $s(\mu)$  is the vertical displacement of the top port of  $\text{arch}_1$ . The system has 60 parameters in total; note, however, that in this system  $\mathcal{D}^{\text{geo}}$  is a strict subset of  $\Pi_{1 \leq i \leq I} \hat{\mathcal{D}}_{\mathcal{M}(i)}^{\text{geo}}$  since all the pillars in the third layer must be of the same length  $\mu_1^{\text{geo}}$ .

For our first analysis we set pillar parameters for the first layer to

$$\begin{aligned} \mu_{\text{pillar}_1} &\equiv (0.6; 1, 10^{-7}), & \mu_{\text{pillar}_2} &\equiv (0.8; 1, 10^{-7}), & \mu_{\text{pillar}_3} &\equiv (1.2; 1, 10^{-7}), \\ \mu_{\text{pillar}_4} &\equiv (1.0; 1, 10^{-7}), & \mu_{\text{pillar}_5} &\equiv (0.8; 1, 10^{-7}), & \mu_{\text{pillar}_6} &\equiv (0.6; 1, 10^{-7}); \end{aligned} \quad (7.14)$$

all pillar parameters in the third layer are set to

$$\mu_{\text{pillar}_7} = \mu_{\text{pillar}_8} = \mu_{\text{pillar}_9} = \mu_{\text{pillar}_{10}} = \mu_{\text{pillar}_{11}} = \mu_{\text{pillar}_{12}} \equiv (1.2; 1, 10^{-7}); \quad (7.15)$$

all the arch parameters are set to  $\mu_{\text{arch}} = (0.2, 10^{-7})$ . (The situation is depicted in Fig. 12). We apply (clamped) zero Dirichlet boundary conditions on all the bottom ports of all the pillars on the bottom (foundation) layer, as well as on the four arch ports on the extreme left and extreme right sides of the structure.

The displacement field of the structure is shown in Figure 13A. The associated RBE system output is  $\tilde{s}(\mu) = -5.65 \times 10^{-5}$ . We obtained the field output bound  $\Delta^{\text{U}}(\mu) = 1.537 \times 10^{-7}$  and the system output error bound  $\Delta^s = 9.72 \times 10^{-8}$ . The true field error is  $\|\mathbb{U}(\mu) - \tilde{\mathbb{U}}(\mu)\|_2 = 4.47 \times 10^{-9}$ : the effectivity of the error bound is  $\Delta^{\text{U}}(\mu) / \|\mathbb{U}(\mu) - \tilde{\mathbb{U}}(\mu)\|_2 = 34.38$ , which is very good; we can further improve this result to  $\Delta_*^{\text{U}}(\mu) / \|\mathbb{U}(\mu) - \tilde{\mathbb{U}}(\mu)\|_2 = 17.43$ . The Online computation time in this case is 0.47 s, with  $\tau_{\text{sc}}^{\text{RB}} = 0.30$  s and  $\tau_{\text{S}}^{\text{RB}} = 0.17$  s. The truth solution computed *via* the truth static condensation approach of Section 3.2 requires computation time of  $\tau_{\text{sc}}^{\text{FE}} = 46$  s. The static condensation system is of size  $n_{\text{sc}} = 440$  – compared to  $\dim(X^h) = 23208$ .

We next demonstrate a “parameter sweep”: we predict the field and output of our system as we vary the height  $\tilde{H}$  of (all) the pillars in the third layer from 0.1 to 2.0; we hold all the other parameters fixed per (7.14), (7.15)

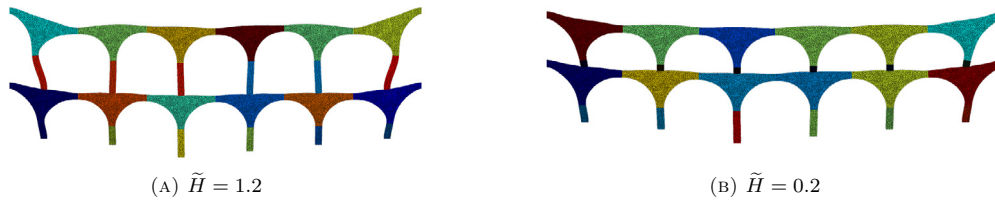


FIGURE 13. Displacement field of the bridge for different values of the height  $\tilde{H}$  of (all) the pillars in the third layer; the displacement field is scaled by a factor of 40000.

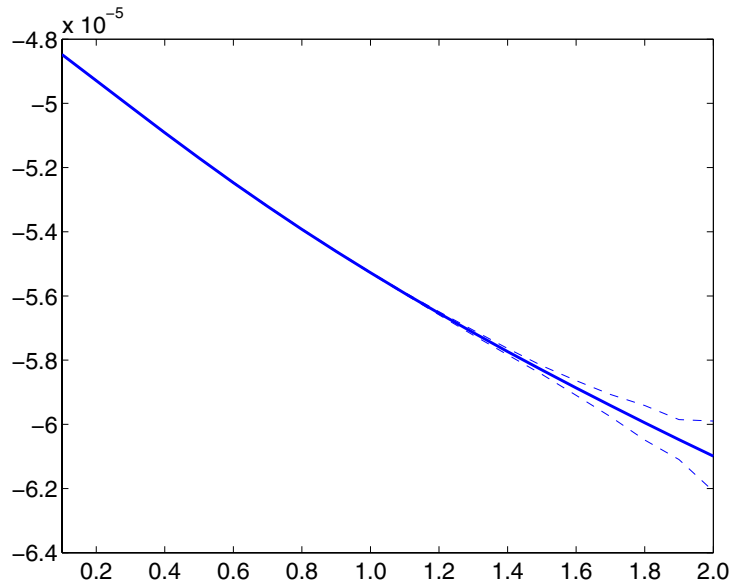


FIGURE 14. Plot of  $\tilde{s}(\mu)$  (solid line) and error bounds (dashed lines) at 20 evenly spaced values of  $\tilde{H}$ .

and  $\mu_{\text{arch}} = (1, 10^{-7})$ . Note that we have  $I_{\text{eff}} = I'_{\text{var}} = 1$  in this example because the pillars in the third layer constitute a single clone set. We show two displacement fields for two different values of  $\tilde{H}$ ,  $\tilde{H} = 1.2$  and  $\tilde{H} = 0.2$ , in Figure 13. We present in Figure 14 the output  $\tilde{s}(\mu)$  and associated error bounds at 20 parameter values in the range  $[0.1, 2.0]$ . Since  $I_{\text{eff}} = 1$ ,  $\tau_{\text{sc}}^{\text{RB}}$  is now reduced to only 0.03 s for each new value of the sweep parameter, while we still have  $\tau_S^{\text{RB}} = 0.17$  s.

For our final example, we consider a  $\text{System}_2$  which is the same structure as in Figure 12, except now we disconnect the top part of the second pillar in the third layer,  $\text{pillar}_8$ , from the arch on the fourth layer,  $\text{arch}_8$ , to model a *broken* column. We consider the same parameter values as in (7.14), (7.15) (and  $\mu_{\text{arch}} = (1.0, 10^{-7})$ ) except now  $\mu_{\text{pillar}_7} = (0.1; 1, 10^{-7})$  to represent a column “stub.” Hence in this case we change the component connectivity with respect to  $\text{System}_1$ , and we also only modify a single component’s parameters:  $I_{\text{eff}} = 1$ . We show the displacement field in Figure 15; as expected, the deflections near the broken column are greatly amplified. This example illustrates the ease with which we may consider both parametric and topological variations in design exercises.

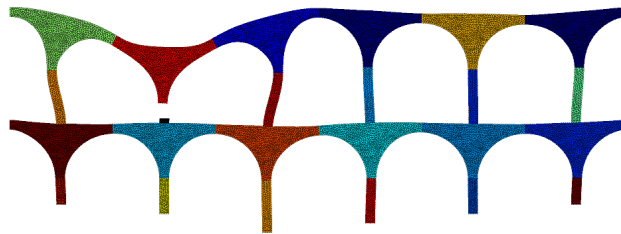


FIGURE 15. Displacement field for the bridge system with one “broken pillar”; the displacement field is scaled by a factor of 10 000.

*Acknowledgements.* This work was supported by OSD/AFOSR/MURI Grant FA9550-09-1-0613, by ONR Grant N00014-11-0713, and by the MIT-Singapore International Design Center. We thank Prof. Hetmaniuk of University of Washington for providing helpful comments and for identifying several important references to prior work. We thank the referees for many suggestions which greatly improved the paper as regards both content and presentation. We thank Dr. Jens Eftang for a careful reading of the manuscript and insights into ongoing extensions.

## REFERENCES

- [1] H. Antil, M. Heinkenschloss, R.H.W. Hoppe and D.C. Sorensen, Domain decomposition and model reduction for the numerical solution of PDE constrained optimization problems with localized optimization variables. *Comput. Visualization Sci.* **13** (2010) 249–264.
- [2] H. Antil, M. Heinkenschloss and R.H.W. Hoppe, Domain decomposition and balanced truncation model reduction for shape optimization of the Stokes system. *Optim. Methods Softw.* **26** (2011) 643–669, doi: 10.1080/10556781003767904.
- [3] J.K. Bennighof and R.B. Lehoucq. An automated multilevel substructuring method for eigenspace computation in linear elastodynamics. *SIAM J. Sci. Comput.* **25** (2004) 2084–2106.
- [4] A. Bermúdez and F. Pena, Galerkin lumped parameter methods for transient problems. *Int. J. Numer. Methods Eng.* **87** (2011) 943–961, doi: 10.1002/nme.3140.
- [5] P. Binev, A. Cohen, W. Dahmen, R. DeVore, G. Petrova and P. Wojtaszczyk, *Convergence rates for greedy algorithms in reduced basis methods*. Technical Report, Aachen Institute for Advanced Study in Computational Engineering Science, preprint: AICES-2010/05-2 (2010).
- [6] F. Bourquin, Component mode synthesis and eigenvalues of second order operators: discretization and algorithm. *ESAIM: M2AN* **26** (1992) 385–423.
- [7] S.C. Brenner, The condition number of the Schur complement in domain decomposition. *Numer. Math.* **83** (1999) 187–203.
- [8] A. Buffa, Y. Maday, A.T. Patera, C. Prud’homme and G. Turinici, *A priori* convergence of the greedy algorithm for the parametrized reduced basis. To appear in *ESAIM: M2AN* (2010).
- [9] Y. Chen, J.S. Hesthaven and Y. Maday, A Seamless Reduced Basis Element Methods for 2D Maxwell’s Problem: An Introduction, edited by J. Hesthaven and E.M. Rønquist, in *Spectral and High Order Methods for Partial Differential Equations-Selected papers from the ICASOHOM’09 Conference* **76** (2011).
- [10] R. Craig and M. Bampton, Coupling of substructures for dynamic analyses. *AIAA J.* **6** (1968) 1313–1319.
- [11] J.L. Eftang, D.B.P. Huynh, D.J. Knezevic, E.M. Rønquist and A.T. Patera, Adaptive port reduction in static condensation, in *MATHMOD 2012 – 7th Vienna International Conference on Mathematical Modelling* (2012) (Submitted).
- [12] M. Ganesh, J.S. Hesthaven and B. Stamm, *A reduced basis method for multiple electromagnetic scattering in three dimensions*. Technical Report 2011-9, Scientific Computing Group, Brown University, Providence, RI, USA (2011).
- [13] G. Golub and C. van Loan, *Matrix Computations*. Johns Hopkins University Press (1996).
- [14] B. Haggblad and L. Eriksson, Model reduction methods for dynamic analyses of large structures. *Comput. Struct.* **47** (1993) 735–749.
- [15] U.L. Hetmaniuk and R.B. Lehoucq, A special finite element method based on component mode synthesis. *ESAIM: M2AN* **44** (2010) 401–420.
- [16] T.Y. Hou and X.-H. Wu, A multiscale finite element method for elliptic problems in composite materials and porous media. *J. Comput. Phys.* **134** (1997) 169–189.
- [17] W.C. Hurty, On the dynamic analysis of structural systems using component modes, in *First AIAA Annual Meeting*. Washington, DC, AIAA paper, No. 64-487 (1964).
- [18] D.B.P. Huynh, G. Rozza, S. Sen and A.T. Patera, A successive constraint linear optimization method for lower bounds of parametric coercivity and inf-sup stability constants. *C. R. Math.* **345** (2007) 473–478.
- [19] L. Iapichino, Quarteroni and G.A., Rozza, A reduced basis hybrid method for the coupling of parametrized domains represented by fluidic networks. *Comput. Methods Appl. Mech. Eng.* **221-222** (2012) 63–82.

- [20] H. Jakobsson, F. Beingzon and M.G. Larson, Adaptive component mode synthesis in linear elasticity. *Int. J. Numer. Methods Eng.* **86** (2011) 829–844.
- [21] S. Kaulmann, M. Ohlberger and B. Haasdonk, A new local reduced basis discontinuous galerkin approach for heterogeneous multiscale problems. *C. R. Math.* **349** (2011) 1233–1238.
- [22] B.S. Kirk, J.W. Peterson, R.H. Stogner and G.F. Carey, `libMesh`: A C++ library for Parallel adaptive mesh refinement/coarsening simulations. *Eng. Comput.* **22** (2006) 237–254.
- [23] D.J. Knezevic and J.W. Peterson, A high-performance parallel implementation of the certified reduced basis method. *Comput. Methods Appl. Mech. Eng.* **200** (2011) 1455–1466.
- [24] Y. Maday and EM Rønquist, The reduced basis element method: Application to a thermal fin problem. *SIAM J. Sci. Comput.* **26** (2004) 240–258.
- [25] Y. Maday, A.T. Patera and G. Turinici, *A priori* convergence theory for reduced-basis approximations of single-parameter elliptic partial differential equations. *J. Sci. Comput.* **17** (2002) 437–446.
- [26] N.C. Nguyen, A multiscale reduced-basis method for parametrized elliptic partial differential equations with multiple scales. *J. Comput. Phys.* **227** (2007) 9807–9822.
- [27] C. Prud’homme, D. Rovas, K. Veroy, Y. Maday, A.T. Patera and G. Turinici, Reliable real-time solution of parametrized partial differential equations: Reduced-basis output bounds methods. *J. Fluids Eng.* **124** (2002) 70–80.
- [28] G. Rozza, D.B.P. Huynh and A.T. Patera, Reduced basis approximation and *a posteriori* error estimation for affinely parametrized elliptic coercive partial differential equations. *Arch. Comput. Methods Eng.* **15** (2008) 229–275.